Journal of Organometallic Chemistry 902 (2019) 120965

Contents lists available at ScienceDirect

Journal of Organometallic Chemistry

journal homepage: www.elsevier.com/locate/jorganchem

Review

Chemistry of macrocyclic tetracarbene complexes: Synthesis, structure, reactivity and catalytic application

Ahmed Hassoon Mageed

Department of Chemistry, Faculty of Science, University of Kufa, P.O. Box 21, Najaf, 54001, Iraq

A R T I C L E I N F O

Article history:
Received 9 August 2019
Received in revised form
25 September 2019
Accepted 28 September 2019
Available online 3 October 2019

Keywords:
Macrocyclic ligands
N-heterocyclic carbene
Transition metals
Catalyst

A B S T R A C T

A narrow area of macrocyclic ligands, including *N*-heterocyclic carbene (NHC) groups and their metal complexes, is reported in the review. This review highlights recent perspectives in the fields of synthesis and structures of mononuclear macrocyclic NHC metal complexes and their catalytic applications. The review covers some transition metals (Cr, Fe, Co, Ni, Rh, Ru, Pd, Pt and Au) and group 13 and 14 metals (Sn, In and Al) with a limited number of macrocyclic tetra-NHC ligands.

Contents

1. Introduction

In 1968, the first *N*-heterocyclic carbene (NHC) complexes were reported by Öfele and Wanzlick [1,2]. Since that time, many NHC-metal complexes have been synthesized [3–16]. NHCs have excellent properties such as σ-donor ability and bonding to both main group and transition metals with better thermal stability than phosphines [17–20]. Nowadays, due to their significant properties, NHCs are used widely as ligands with hard and soft transition metals.

A few examples of macrocyclic tetra-NHC ligands and their metal complexes have been investigated [8,9,12]. In 2005, the first macrocyclic tetra–NHC–Pt^{II} complex was synthesized by Hahn's group [21,22]. After two years, Murphy's group synthesized 24-atom

E-mail address: ahmedh.alameri@uokufa.edu.iq.

https://doi.org/10.1016/j.jorganchem.2019.120965
0022-328X/

List of abbreviations

An isomer shift δ
1,2-bis(diphenylmethylene)hydrazine DPH
cyclo-tri-tert-butylphosphine cyclo-$(PtBu)_3$
Density functional theory DFT
Diazodiphenylmethane N_2CPh_2
Dimethylformamide DMF
2,6-Diisopropylphenyl azide DiPP-azide
Electrospray ionization mass spectrometry ESI-MS
N-heterocyclic carbene NHC
High-resolution direct analysis in real-time HR-DART/MS mass spectrometry
Ligand metal charge transfer LMCT
Lithium diisopropyl amide LDA
Nuclear magnetic resonance NMR
Platinum(II) acetylacetonate $Pt(acac)_2$
P-tert-butyl-dibenzo-7λ^3phosphanorbornadiene ^{t}BuPA
Quadrupole splitting ΔEq
Superconducting quantum interference device SQUID
2-(tert-butylsulfonyl)iodosylbenzene (2-(tBuSO$_2$)-C_6H_4IO)
tert-Butyl isocyanide CN^tBu
Tetraphenylethene TPE
Trimethylsilyl azide TMS-azide
Tris(4-bromophenyl)-ammoniumyl hexachloroantimonate $[N(C_6H_4\text{-}4\text{-}Br)_3]SbCl_6$
Trityl S-nitrosothiol Ph_3CSNO
Triphenylphosphine PPh_3

ringed macrocyclic ligand with its corresponding Ag^I, Cu^I and Pd^{II} complexes [23]. In 2009, Murphy and coworkers reported the first macrocyclic tetra−NHC−Co^{II} complex, which is used as catalytic application in the reduction of aryl halides [24]. In 2010, the same group synthesized the first macrocyclic tetra−NHC−Ni^{II} complex, which is worked successfully as a catalyst to reduce organic substrates [25], such as the Birch reduction of aromatic rings and reductions of carbonyl compounds [26–31]. In 2011, Jenkins and coworkers reported the first macrocyclic tetra−NHC−Fe^{II} complex, which is discovered to be aziridination catalyst [32,33]. In 2012, the first macrocyclic tetracarbene Cr^{III}, Au^{III}, Rh^{III}, and Ru^{II} complexes were reported by the same group [33].

Recently, several macrocyclic NHCs with its corresponding metal complexes such as Fe [8,34–36], Ni [37,38] and Pd [37,38] were reported with catalytic applications. However, there are a limited number of macrocyclic tetra-NHC metal complexes such as Ru, Rh, Ir and Au which have been reported. All published synthetic protocols and structures of mononuclear metal complexes with macrocyclic tetra-NHC ligands and their catalytic applications are reported. In our knowledge, some recent reviews partly touched on the subject of this review, however, no review has covered the synthesis and structures of all transition metal complexes with macrocyclic tetra-NHC ligands.

2. Macrocyclic tetra-NHC metal complexes

2.1. Chromium

In 2012, the first macrocyclic tetra-NHC chromium complex was reported by Jenkins and coworkers [33]. The mononuclear Cr^{III} complex **2**−PF_6 was formed by transmetalation reaction using $CrCl_2$ and Ag^I complex **1**–4(PF_6) in yield 58% (Scheme 1). The trivalent oxidation state of the complex was confirmed by ESI-MS characterization.

The X-ray diffraction studies for **2**−PF_6 showed that the NHC units and two Cl^- ligands occupy equatorial and axial coordination sites, respectively, with Cr-$C_{equatorial}$ distances are between 2.09 and 2.14 Å and Cr-Cl_{axial} being around 2.35 Å (Table 1 and Fig. 1). Cyclovoltammetric studies of **2**−PF_6 showed two redox potentials, at +1.31 V and −1.99 V [33].

Recently, Jenkins and coworkers reported the first example of aziridination catalysis with **2**−PF_6 [39]. The complex **2**−PF_6 reacted with aryl azides and a series of substituted aliphatic alkenes to obtain C_2 + N_1 aziridination in yields (26–41%) (Scheme 2). The complex **2**−PF_6 was the most effective catalyst for aliphatic alkenes at low loading to date [39].

In 2017, the group of Jenkins synthesized new tetra−NHC−Cr^{II} complex **3** which was supported by NHC-borate macrocycle (Scheme 3) [40]. The X-ray studies showed that **3** was square planar. Cr−C distances are in the range 2.076(3) −2.132(3) Å (Table 1). The high reactivity of **3** toward some organic azides and Me_3NO led to form a series of tetra−NHC−Cr^{IV} complexes [40]. The oxidation of **3** with Me_3NO formed Cr^{IV}-oxo complex **4** in moderate yield 50%. The crystal structure of **4** was a square pyramidal geometry, and the Cr−C bond distances are in the range 2.026–2.094 Å. The reaction of **3** with tolyl azide or n-octyl azide led to Cr^{IV} metallotetrazene complexes (**5** and **6**) in yield 40%. Both crystal structures for **5** and **6** were distorted trigonal prismatic

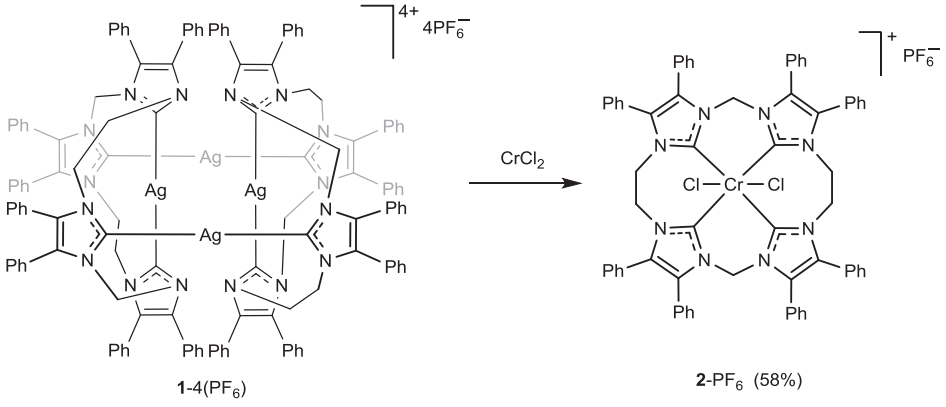

Scheme 1. Synthesis of macrocyclic tetra−NHC−Cr^{III} complex.

Table 1
Selected bond lengths (Å) and angles (°) for Cr complexes.

Complexes	L_1	L_2	Cr–C	Cr-L_1	Cr-L_2	C–Cr–C	L_1-Cr-L_2	Ref.
2–PF_6	Cl	Cl	2.135(5), 2.101(5), 2.142(5), 2.094(6)	2.340(2)	2.356(2)	172.6(2), 170.6(2)	179.3(1)	[33]
3	–	–	2.076(3), 2.132(3)	–	–	170.54(14), 177.39(12)	–	[40]
4	O	–	2.094(5), 2.031(5), 2.080(5), 2.026(5)	1.564(3)	–	153.3(2), 147.7(2)	–	[40]
5	N	N	2.056(3), 2.120(3), 2.063(3), 2.118(3)	1.977(3)	1.964(3)	121.82(11), 140.41(11)	–	[40]
6	N	N	2.0701(19), 2.1288(19), 2.0879(19), 2.1591(19)	1.9644(16)	1.347(2)	141.79 (7), 126.68(7)	–	[40]
7	N	–	2.104(6), 2.097(6), 2.065(6), 2.082(6)	1.703(4)	–	147.81(2), 151.8(2)	–	[40]
8	N	–	2.096(3), 2.101(3), 2.070(3), 2.066(3)	1.686(2)	–	143.9(11), 142.0(11)	–	[40]
9 [a]	N	–	2.086(5), 2.111(4), *2.104(4), 2.163(4)*	1.667(5), *1.896(5)*	–	158.80 (2), 153.4(2), *168.4(2), 160.5(2)*	–	[40]

[a] Normal font for Cr1; *Italics* font for Cr2.

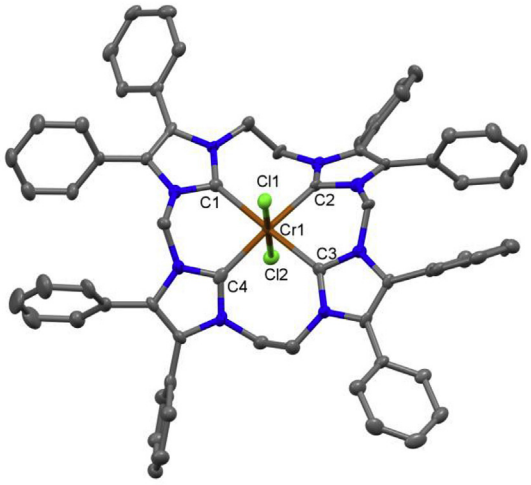

Fig. 1. Crystal structure (50% probability level for the displacement ellipsoids) of the cation of **2**–PF_6.

geometry with the similar Cr–C bond distances are in the range 2.056–2.1591 Å (Fig. 2). The reaction of **3** with less sterically bulky organic azide such as mesityl azide and adamantyl azide formed Cr^{IV} imido complexes (**7** and **8**) in yield 50% and 20%, respectively. The X-ray studies of both complexes showed a square pyramidal geometry with the similar Cr^{IV}-imido bond distances are in the range 1.686–1.704 Å. The reaction of **3** with TMS-azide obtained the first bridging mononitrido of dimeric chromium complex **9** in 50% yield. The X-ray structural studies for **9** showed that the bridging nitrido arranged linearly between the two Cr centers about 180°. The Cr–C bond distances are in the range 2.167–2.082 Å. The suggestion of Cr^{III}/Cr^{IV} mixed valence complex was investigated by the increasing magnetic susceptibility at low temperature. All complexes were characterized by NMR spectroscopy, UV–visible and mass spectrometry [40].

2.2. Iron

2.2.1. Synthesis of iron tetra-NHC complexes

The first macrocyclic tetra–NHC–Fe complex **10**–2(PF_6) was synthesized in low yield 11% by reaction of FeI_2, lithium diisopropyl amide, and the imidazolium salt $\mathbf{L^2}$.4HI [32]. However, **10**–2(PF_6) was also synthesized in high yield 92% by transmetalation using **1**–4(PF_6) and FeI_2 (Scheme 4) [33]. The complex had distorted octahedral geometry having two solvent molecules in axial positions and four NHC in equatorial positions (Table 2) [32,33].

Complexes **11**–2(OTf) and **12**–2(OTf) were synthesized in low yield 30% and 38%, respectively, by the reaction of the macrocyclic imidazolium salts with $[Fe\{N(SiMe_3)_2\}_2]_2$ (Scheme 5) [34,41]. However, **13**–2(PF_6) was synthesized in high yield 93% by using an excess of $[Fe\{N(SiMe_3)_2\}_2]_2$ with the macrocyclic imidazolium salt [42]. The complex **11**–2(OTf) is sensitive to moisture and air. The crystal structures of all complexes were distorted octahedral

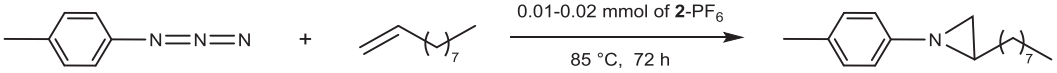

Scheme 2. Aziridination reaction catalyzed by **2**–PF_6.

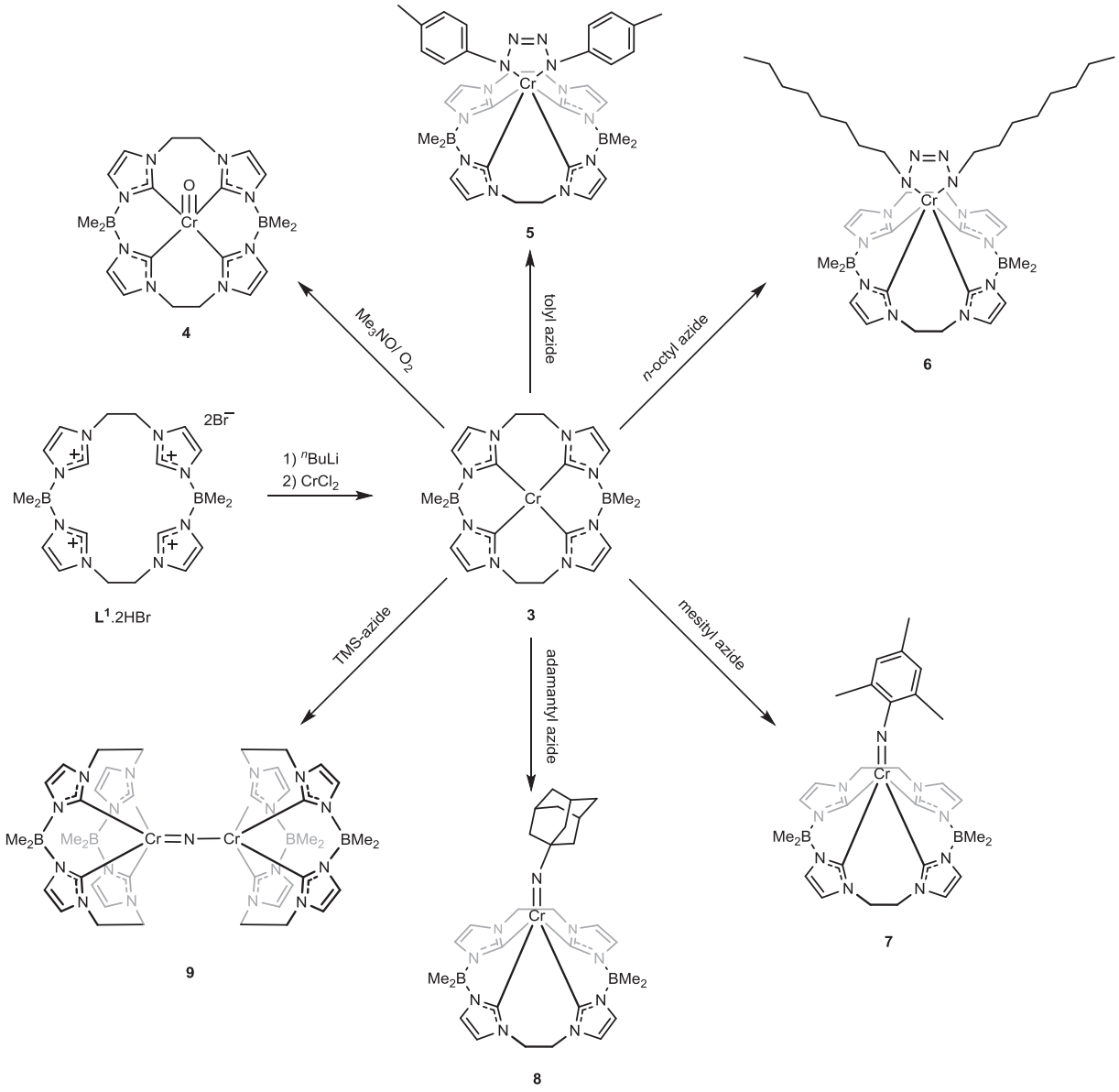

Scheme 3. Synthesis and reactions of Cr^{II} complex.

geometry having two MeCN molecules in axial positions (Table 2 and Fig. 3). The Mössbauer spectrum showed that **11**−2(OTf) and **12**−2(OTf) had the same isomer shift ($\delta = 0.23\ mm\ s^{-1}$), and a similar quadrupole splitting (ΔEq) (**11**−2(OTf): $2.10\ mm\ s^{-1}$; **12**−2(OTf): $2.19\ mm\ s^{-1}$) [34,41]. Cyclovoltammetric studies showed that the **12**−2(OTf) occurred reversible oxidation reaction at −0.16 V [34], which is lower voltage than **11**−2(OTf) at +0.03 V and **13**−2(PF_6) at +0.15 V [42].

Complexes **14** and **15** were synthesized in low yield 29% and 25%, respectively, by the reaction of the macrocyclic imidazolium salts (**L**^{6}.2HBr and **L**^{1}.2HBr) with $FeBr_3$ in the presence of ^{n}BuLi (Scheme 6) [35,43]. The X-ray studies for **14** and **15** showed a distorted square pyramidal geometry (Table 2 and Fig. 3). Cyclovoltammetric studies showed that **15** showed reversible reduction reactions at −0.95 V [43]. While, **14** showed an irreversible oxidation at +0.36 V and an irreversible reduction at −1.25 V [35]. Reduction of **15** by sodium amalgam formed **17** in yield 52% [43]. While the complex **16** was synthesized by reaction of **L**^{6}.2HBr with $FeCl_2$ in the presence of ^{n}BuLi in moderate yield 65% (Scheme 6) [35]. Crystal structure for **16** and **17** had a square planar geometry with the average Fe−C bond distances is 1.97 Å. (Table 2).

2.2.2. Reactions of iron tetra-NHC complexes

The reaction of **11**−2(OTf) with an excess (2-(tBuSO$_2$)-C_6H_4IO) formed **18**−2(OTf) in low yield 16% (Scheme 7) [41]. The formation of **18**−2(OTf) was confirmed by ESI-MS. The reaction was monitored by UV/Vis spectroscopy at −40 °C, displaying a broader band at around 400 nm. Normally, The typical chromophore of oxoiron(IV) is absorption between 700 and 900 nm. This reaction was completed after nearly 2 h. Crystals of the **19**−2(OTf) were grown by slow diffusion of vapours between neat diethyl ether and a solution of the **18**−2(OTf) in EtCN (Scheme 7). The result of X-ray diffraction studies of the **19**−2(OTf) is similar to that seen in the **18**−2(OTf), with the oxygen atom and the EtCN ligand in the axial coordination (Table 2) [41].

The formation of complex **20**−4(OTf) was accomplished by decomposition of **18**−2(OTf) at room temperature. The complex **20**−4(OTf) was also formed, in high yield 98%, by direct oxidation of

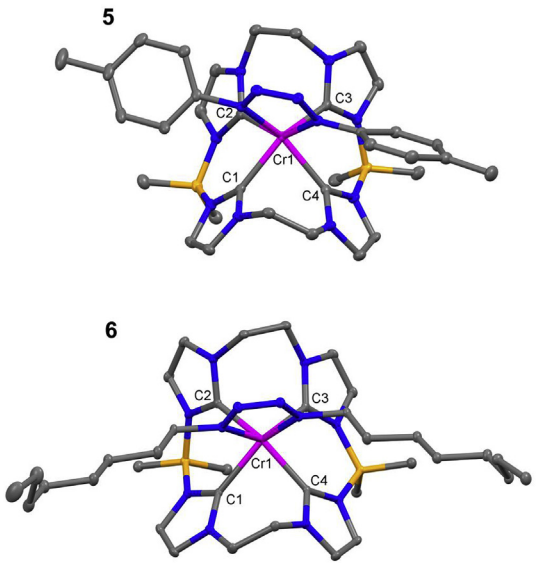

Fig. 2. Crystal structures (30% probability level for the displacement ellipsoids) of **5** and **6**.

11–2(OTf) with *m*-CPBA, trimethylamine N-oxide, C_6H_5IO, or with dioxygen in acetonitrile [41]. **21**–4(OTf) was formed by oxidation of **12**–2(OTf) with air (Scheme 7) [34]. In both complexes, the coordination sphere of each Fe^{III} centre is square-pyramidal geometry, having four Fe–C bonds (Table 2 and Fig. 4), and one Fe–O bond (Fe–O ~1.75 Å). The Mössbauer spectrum showed an isomer shift (δ) (**20**–4(OTf): 0.04 mm s^{-1}, **21**–4(OTf): 0.03 mm s^{-1}), and a quadrupole splitting (ΔEq) (**20**–4(OTf): 2.56 mm s^{-1}; **21**–4(OTf): 2.60 mm s^{-1}), that are extremely similar in both cases. Both complexes **20**–4(OTf) and **21**–4(OTf) were also confirmed by mass spectrometry, UV–visible spectroscopy, and SQUID measurements [34,41].

The oxidation of **11**–2(OTf) with $[N(C_6H_4\text{-}4\text{-}Br)_3]SbCl_6$ led to **22**–3($SbCl_6$) at −35 °C and had an oxidation wave at +0.67 V in MeCN (Scheme 7) [34]. The structure of **22**–3($SbCl_6$) is extremely similar to that seen in **11**–2(OTf) (Table 2). The slow crystallization of mixture between **11**–2(OTf) and $[N(C_6H_4\text{-}4\text{-}Br)_3]SbCl_6$ at 3 °C led to **23**–2(OTf) in good yields (75%). **23**–2(OTf) was also synthesized by reacting $[^nBu_4N]Cl$ with a solution of **22**–3($SbCl_6$) in MeCN (Scheme 7). The structure had a square pyramidal geometry, with the Cl^- ligand in axial coordination site (Fe–Cl = 2.27 Å). The complex **22**–3($SbCl_6$) had a low spin state (S = ½) with an isomer shift (δ = 0.09 mm s^{-1}) and a quadrupole splitting (ΔEq = 0.63 mm s^{-1}), which was confirmed by Mössbauer spectroscopy. The complex **23**–2(OTf) had a low spin state (S = 3/2) with an isomer shift (δ = 0.11 mm s^{-1}) and a quadrupole splitting (ΔEq = 4.52 mm s^{-1}) [34]. Mixing a solution of **12**–2(OTf) in DCM with AgOTf led to the red product of **24-**2(OTf) (Scheme 7). Its structure was similar to that seen in the **23**–2(OTf). SQUID measurements showed the low-spin state (S = 3/2) of **24**–2(OTf) (1.97 cm^3 K mol^{-1}). An isomer shift (δ = 0.16 mm s^{-1}) with a quadrupole splitting (ΔEq = 5.02 mm s^{-1}) for **24**–2(OTf) was shown by the Mössbauer spectrum. Adding MeCN to a solution of **24**–2(OTf) in DCM formed **25**–3(OTf) (Scheme 7). Grown crystal of **25**–3(OTf)

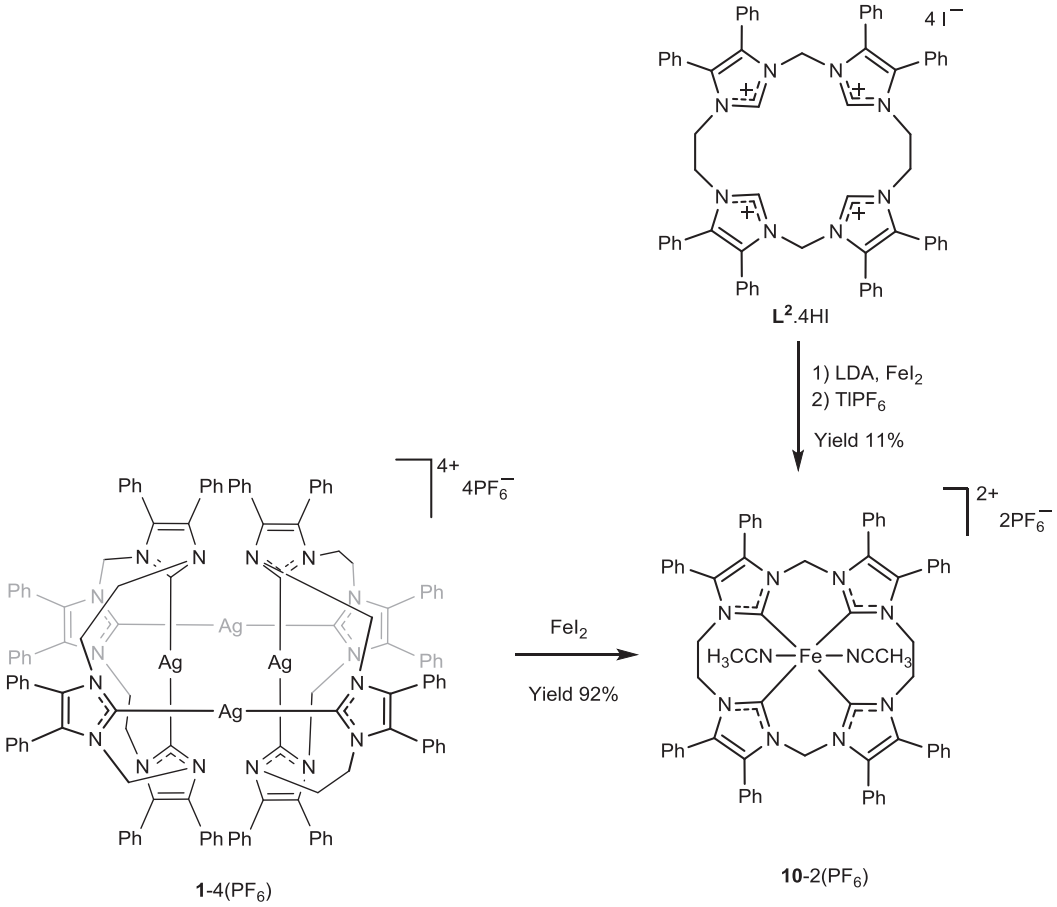

Scheme 4. Synthesis macrocyclic tetra–NHC–Fe^{II} complex **10**–2(PF_6).

Table 2
Selected bond lengths (Å) and angles (°) for Fe complexes.

Complexes	L_1	L_2	Fe—C	Fe-L_1	Fe-L_2	C—Fe—C	L_1-Fe-L_2	Ref.
10—2(PF_6)	MeCN	MeCN	2.052(2), 1.986(2), 2.029(2), 1.977(2)	1.931(2)	1.917(2)	169.7(1), 172.68(1)	178.2(1)	[32,33]
12—2(OTf)	MeCN	MeCN	1.969(5), 1.973(5), 2.033(5), 2.038(5)	1.920(4)	1.921(4)	176.8(2), 171.75(19)	176.86(18)	[34]
13—2(PF_6)	MeCN	MeCN	1.912(3), 1.905(3), 1.909(3), 1.902(3)	1.930(1)	1.933(1)	178.3(1), 179.6(1)	177.08(3)	[42]
14	Br	—	1.989(4), 1.983(4)	2.4493(9)	—	155.3(1)	—	[35]
15	Br	—	2.055(1), 2.045(1), 2.028(1), 2.019(1)	2.5016(2)	—	152.5(1), 153.8(1)	—	[43]
16	—	—	1.943(3), 1.941(3), 1.934(3), 1.941(3)	—	—	179.2(1), 178.3(1)	—	[35]
17	—	—	2.017(4), 2.003(4), 1.975(5), 1.964(5)	—	—	174.9(1), 179.6(1)	—	[43]
19—2(OTf)	O	MeCN	1.979(5), 1.980(5), 2.037(5), 2.045(5)	1.661(3)	—	174.00(19), 172.92(19)	176.65(17)	[41]
20—4(OTf)	O	—	1.970(4), 1.973(4), 2.028(4), 2.036(4), 1.947(4), 1.982(4), 2.012(4), 2.020(4)	1.752(2)	—	—	—	[41]
22—3($SbCl_6$)	MeCN	MeCN	1.986(4), 1.995(4), 2.044(4), 2.053(4)	1.923(3)	1.934(3)	174.94(15), 174.23(15)	177.22(13)	[34]
23—2(OTf)	Cl	—	1.979(5), 2.062(5), 1.992(6), 2.002(5)	2.2656(9)	—	158.3(3), 169.1(2)	—	[34]
24—2(OTf)	OTf	—	1.979(5), 1.984(5), 2.030(5), 2.037(5)	2.034(3)	—	155.66(19), 157.44(19)	—	[34]
26—2(OTf)	NO	—	1.963(3), 2.014(3), 1.964(3), 2.033(3)	1.670(3)	—	164.33(14), 148.10(14)	—	[44]
27—2(PF_6)	NO	—	1.950(3), 1.952(3), 1.936(3), 1.939(3)	1.673(2)	—	152.7(1) 152.5(1)	—	[42]
28—OTf	NO	—	1.928(2), 1.952(2), 1.991(2), 2.001(2)	1.660(2)	—	153.84(9), 140.61(9)	—	[46]
29—2(OTf)	NO	ONO	1.984(4), 1.988(4), 2.012(4), 2.047(4)	1.625(4)	1.979(3)	171.84(15), 172.12(17)	175.62(13)	[46]
31—2(PF_6)	SMe_2O	SMe_2O	1.936(3), 1.938(3)	2.205(1)	2.205(1)	180	180	[42]
32—2(PF_6)	CO	CO	1.915(3), 1.913(3), 1.914(4), 1.916(4)	1.826(1)	1.815(3)	179.3(2), 177.7(2)	177.1(2)	[42]
33—2(PF_6)	N	N	1.952(3), 1.987(3),	1.896(2)	1.921(2)	136.3(1) 125.4(1)	—	[47]

Table 2 (*continued*)

Complexes	L_1	L_2	Fe–C	Fe-L_1	Fe-L_2	C–Fe–C	L_1-Fe-L_2	Ref.
34–PF_6	N	N	1.954(3), 2.011(2) 1.963(3), 1.963(3), 1.976(3), 1.958(3)	1.947(2)	1.980(2)	147.8(1) 118.1(1)	–	[47]
38	O	–	1.966(2), 1.963(2), 1.969(2), 1.970(2)	1.731(2), 1.730(2)	–	–	–	[35]
39	N	–	1.9331(14), 1.9293(13), 1.9868(14), 1.9963(14)	1.6552(12)	–	143.06(6), 141.19(6)	–	[36]
41	N	–	1.9865(14), 1.9802(13), 1.9730(13), 1.9784(14)	1.7300(12)	–	150.83(6), 152.80(6)	–	[36]

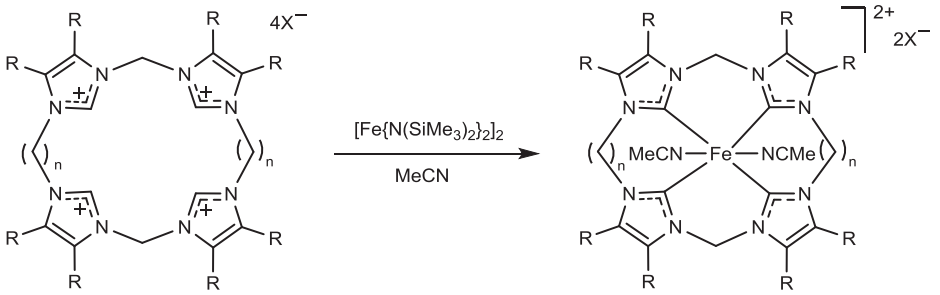

L^3.4HX (R = H, X = OTf, n = 2)
L^4.4HX (R = Me, X = OTf, n = 2)
L^5.4HX (R = H, X = PF_6, n = 1)

11-2(X) (R = H, X = OTf, n = 2), 30%
12-2(X) (R = Me, X = OTf, n = 2), 38%
13-2(X) (R = H, X = PF_6, n = 1), 93%

Scheme 5. Synthesis of complexes **11**–2(OTf) - **13**–2(PF_6).

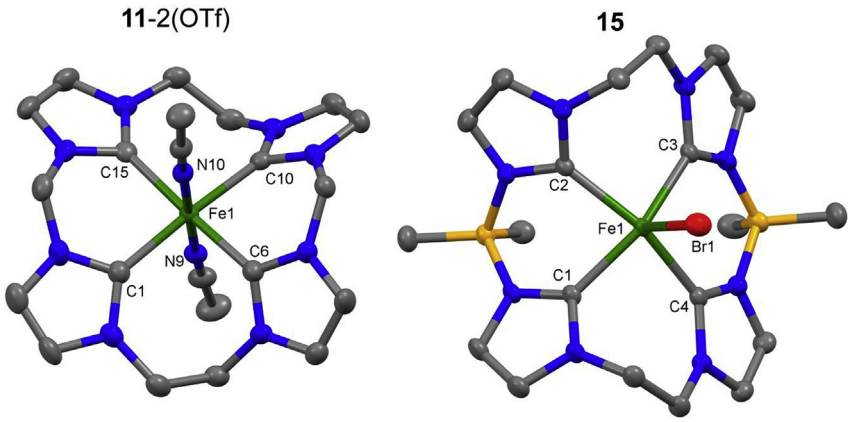

Fig. 3. Crystal structures (50% probability level for the displacement ellipsoids) of the cations of **11**–2(OTf) and **15**.

was unsuccessful because the complex is decomposed readily in solution [34].

The reaction of **11**-2(OTf) with trityl S-nitrosothiol obtained **26**–2(OTf) in yield 54% [44]. The complex **27**–2(PF_6) was also formed, in yield 73%, by the reaction of **13**–2(PF_6) with nitric oxide (Scheme 8) [42]. **26**–2(OTf) was stable in solid state, but, decomposed in solution. The crystal structure of both **26**–2(OTf) and **27**–2(PF_6) showed a distorted square pyramidal geometry, with four NHC units in equatorial coordination sites and one NO ligand in axial coordination site (Table 2) [42,44]. SQUID measurements confirmed the low-spin state ($S = ½$) of **26**–2(OTf) ($0.39\ cm^3\ K\ mol^{-1}$). A low isomer shift ($\delta = -0.01\ mm\ s^{-1}$) with a large quadrupole splitting ($\Delta Eq = 2.36\ mm\ s^{-1}$) for **26**–2(OTf) was shown by the Mössbauer spectrum. Furthermore, an isotopic triplet at $g_{iso} = 2.027$ with hyperfine coupling A ($^{14}N_{NO}$) = 13.4 G was showed by X-band EPR spectroscopy. The UV/vis/near infrared spectrum revealed absorption bands around 350 nm (ligand-to-metal-charge-transfer (LMCT) from NHCs to Fe) and 615 nm (LMCTs

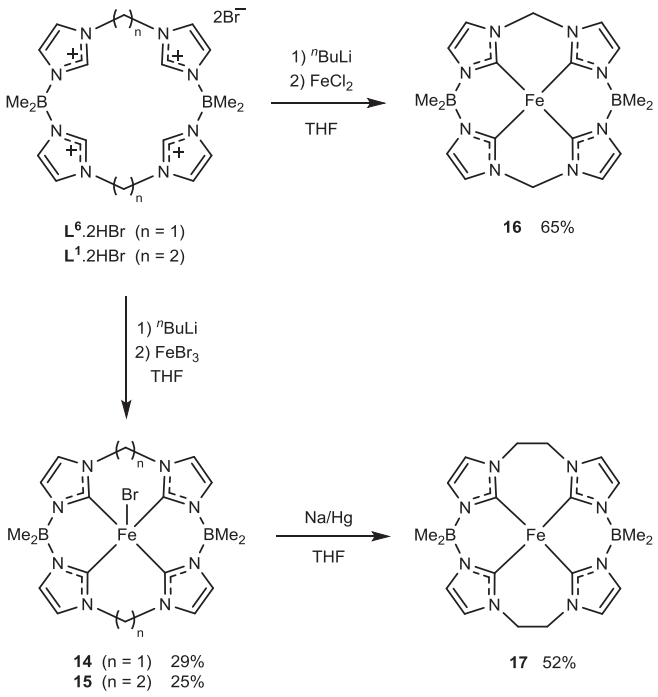

Scheme 6. Synthesis of complexes **14**–**17**.

from NO to Fe), which is assigned by DFT. The IR spectrum of **26**–2(OTf) displayed a ν_{N-O} absorption at 1748 cm^{-1}, which is higher energy than those seen in low-spin $(FeNO)^7$ complexes (1600–1700 cm^{-1}) [45]. Based on the DFT calculations, the singly occupied molecular orbital (SOMO) of **26**–2(OTf) had a mostly iron character (53% Fe and 10% NO ligand). Cyclovoltammetric studies showed that the **26**–2(OTf) showed reversible reduction reactions at −0.98 V in acetonitrile [44], while Kühn and coworkers reported that **27**–2(PF_6) showed an irreversible reduction at −1.06 V [42].

The reduction of **26**–2(OTf) with cobaltocene obtained **28**–OTf in yield 47%. The oxidation of **11**–2(OTf) or **26**–2(OTf) with NO in the presence of O_2 led to **29**–2(OTf) in yield 63% (Scheme 8) [46]. The crystal structure of **28**–OTf had a distorted square pyramidal geometry. For complex **29**–2(OTf), the coordination sphere of the Fe centre is an octahedral geometry with the NO and nitrito-O ligands occupy the apical position. An isomer shift ($\delta = 0.02$ mm s^{-1}) with a quadrupole splitting ($\Delta Eq = 0.85$ mm s^{-1}) for **28**–OTf was shown by the Mössbauer spectrum. For **29**–2(OTf), a low isomer shift ($\delta = -0.16$ mm s^{-1}) with a large quadrupole splitting ($\Delta Eq = 3.12$ mm s^{-1}). Cyclovoltammetric studies showed that the **29**–2(OTf) showed two redox reactions, an irreversible reduction at −0.51 V and a reversible reduction at −1.0 V in acetonitrile.

An excess of DMSO was added to the solution of the **13**–2(PF_6) in acetonitrile to form mono- and bis-DMSO Fe^{II} complexes (**30**–2(PF_6) and **31**–2(PF_6)) [42]. The complex **32**–2(PF_6) obtained by mixing **13**–2(PF_6) under a carbon monoxide pressure of 2.5 atm at 40 °C (Scheme 8) [42]. The crystal structure of **31**–2(PF_6) and **32**–2(PF_6) showed a distorted octahedral geometry with both (DMSO or CO) ligands in axial coordination sites (Table 2). Cyclovoltammetric studies showed that the **32**–2(PF_6) showed quasi-reversible oxidation at 1.25 V [42].

Reaction of tolyl azide with **10**–2(PF_6) at 40 °C formed **33**–2(PF_6) in yield 74% (Scheme 9) [47]. The X-ray studies for **33**–2(PF_6) showed a trigonal prismatic geometry with a slightly distorted twisting (Fig. 5). The Fe–C bond distance is about 1.98 Å [47], which is slightly shorter than those seen in **10**–2(PF_6) and similar to the distance values seen for other complexes (Table 2) [32–34,41,42]. The complex **33**–2(PF_6) with a trigonal prismatic geometry is the first complex reported so far. The complex **33**–2(PF_6) had a low spin state (S = 0) with an isomer shift ($\delta = -0.01$ mm s^{-1}) and a quadrupole splitting ($\Delta Eq = 0.62$ mm s^{-1}), which was confirmed by Mössbauer spectroscopy. Cyclovoltammetric studies showed reversible redox reactions at −1.05 V in acetonitrile. Reaction of **33**–2(PF_6) with cobaltocene obtained **34**-PF_6 (Scheme 9). Its structure was similar to that seen in the **33**–2(PF_6) but, the dihedral angle (φ) had increased to 22.1°. The complex **34**–PF_6 had a low spin state (S = ½) with an isomer shift ($\delta = -0.10$ mm s^{-1}) and a quadrupole splitting ($\Delta Eq = 1.13$ mm s^{-1}), which was confirmed by Mössbauer spectroscopy [47]. The authors reported that **34**–PF_6 showed a perfect catalyst for aziridination as seen in **10**–2(PF_6) [47].

The complex **16** was reacted with MeCN, PPh_3, and CN^tBu to form **35**, **36** and **37**, respectively (Scheme 10) [35]. Cyclovoltammetric studies showed that the **35** showed a reversible redox reaction at −0.71 V. The complex **36** is moisture and air sensitive as its **16**. Dinuclear NHC–Fe^{III} complex **38** was also formed by direct oxidation of **16** with trimethylamine N-oxide or dioxygen in yield 74%. Its structure is similar fashion to that seen in **20**–4(OTf) and **21**–4(OTf) (Table 2) [35]. The complex **16** reacted with some substituted azides at 25C to obtain three Fe^{IV} imides

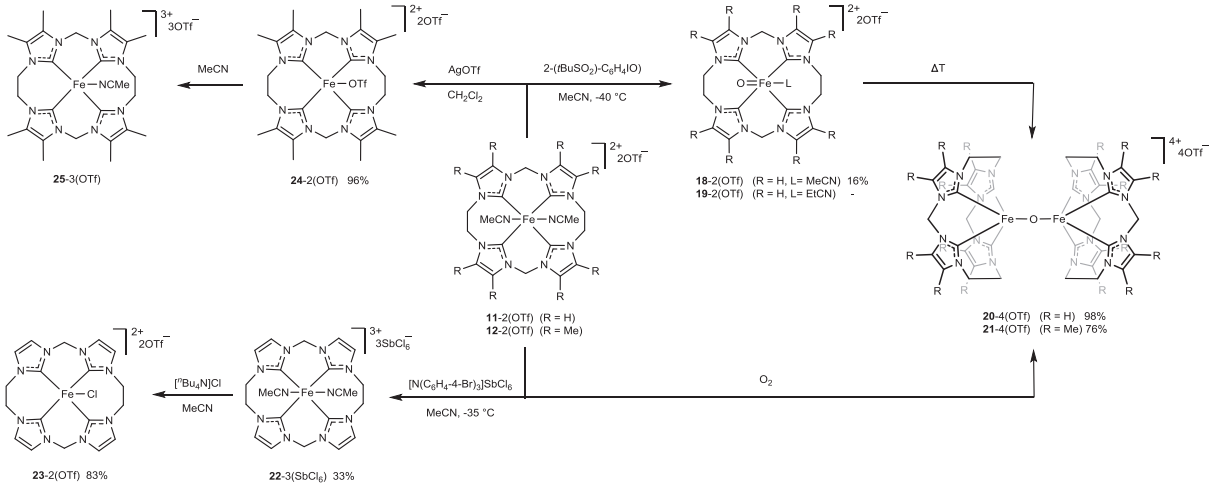

Scheme 7. Reactions of macrocyclic tetra–NHC–Fe complexes.

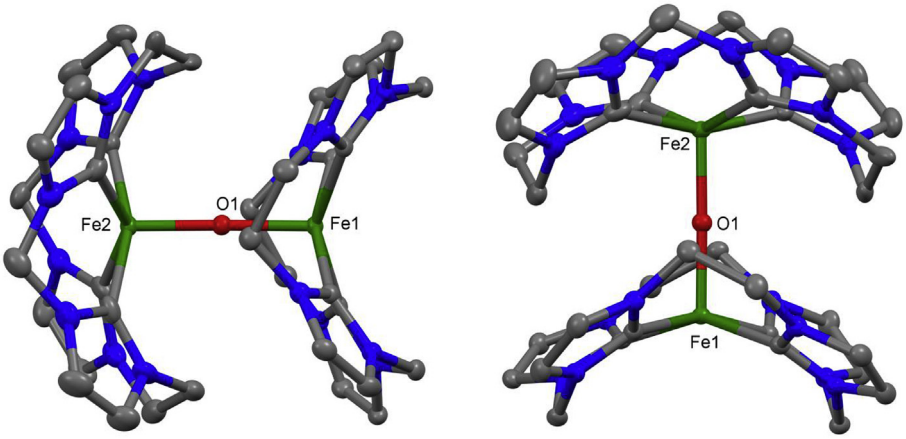

Fig. 4. Crystal structure (30% probability level for the displacement ellipsoids) of the cation of **20**–4(OTf).

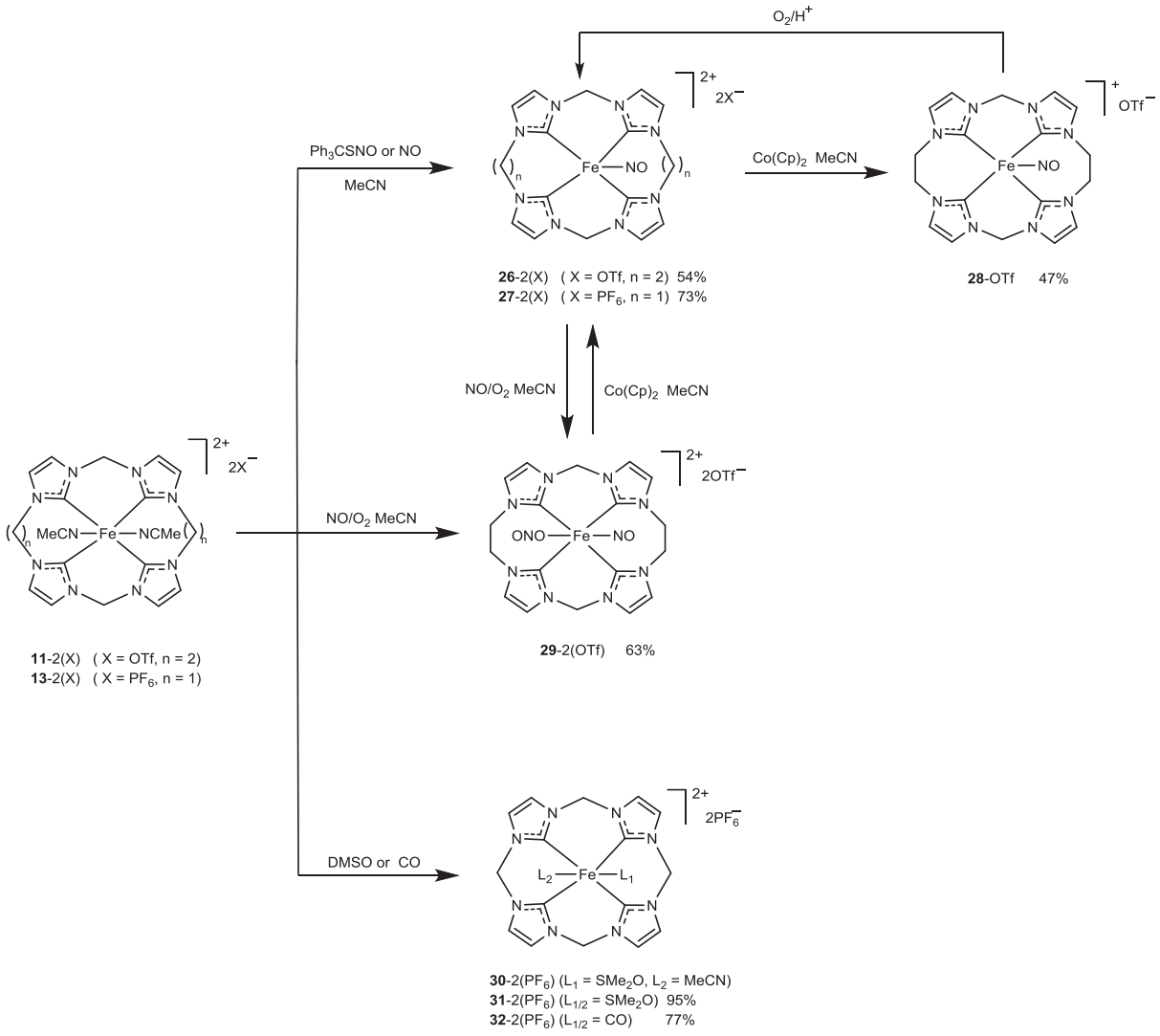

Scheme 8. Reactions of complexes **11**–2(OTf), **13**–2(PF_6) and **26**–2(OTf).

complexes (**39**, **40** and **41**) in high yield (Scheme 10) [36]. The X-ray studies for all complexes showed a distorted square pyramidal geometry having one imide molecule in an axial coordination site in each complex (Table 2). An isomer shift ($\delta = -0.18$ mm s^{-1}) with a quadrupole splitting ($\Delta Eq = 0.97$ mm s^{-1}) for **39** was shown by the Mössbauer spectrum. For **40**, The Mössbauer spectrum was

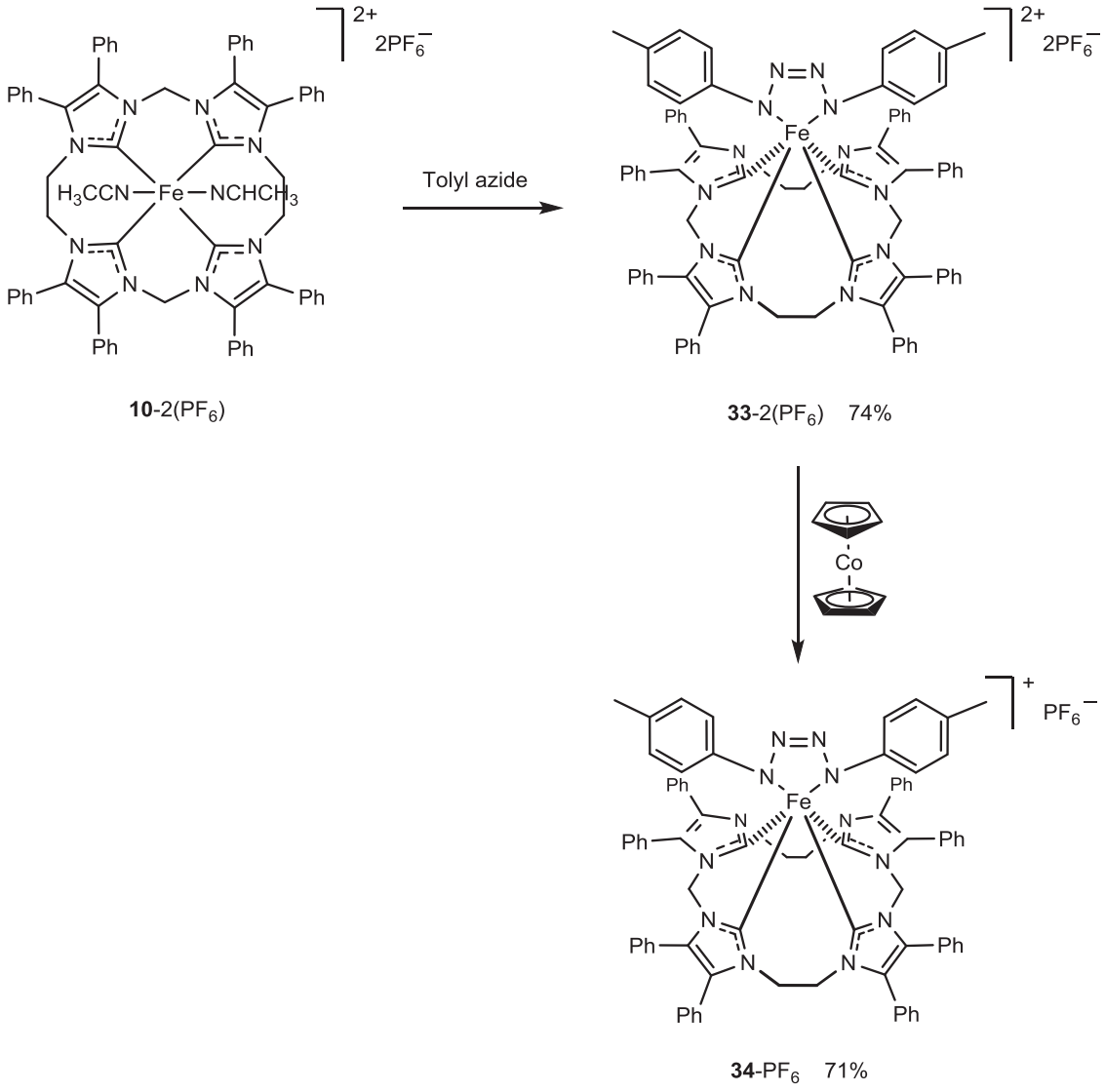

Scheme 9. Reactions of complex **10**−2(PF_6).

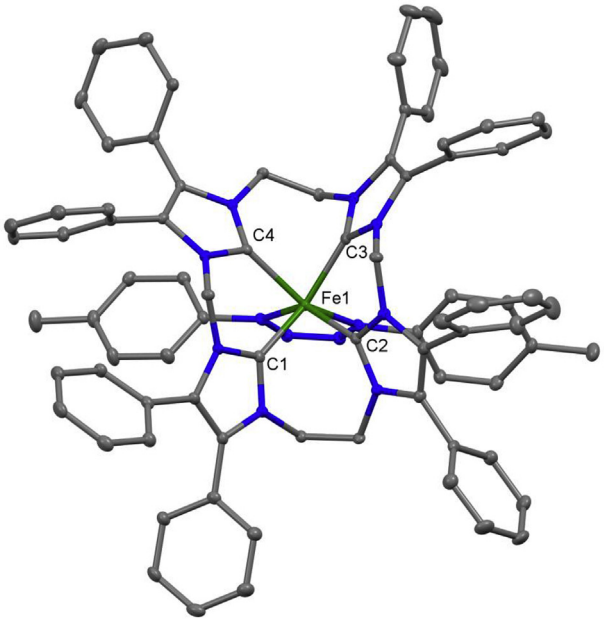

Fig. 5. Crystal structure (30% probability level for the displacement ellipsoids) of the cation of **33**−2(PF_6).

similar to **39**. While **41** showed an isomer shift ($\delta = -0.11$ mm s^{-1}) with a large quadrupole splitting ($\Delta Eq = 2.67$ mm s^{-1}) [36].

2.2.3. Catalytic applications of iron tetra-NHC complexes

The reactions between different aryl azides (1.0 equiv.) and excess alkenes in the presence of **10**−2(PF_6) (0.1−1.0 mol %) at 90 °C for 18 h to obtain aziridines in yields (37−82%) (Scheme 11). Disubstituted alkenes, including *cis*-substituted example, reacted in the presence of **10**−2(PF_6) obtaining high yield 97%. While trisubstituted or tetrasubstituted alkenes also reacted using **10**−2(PF_6) obtaining low yields of 20−39%. The reaction mechanism for aziridination suggests the formation Fe^{IV} imido complex as potential intermediate (Scheme 14) [32].

The complex **16** reacted with N_2CPh_2 to obtain three compounds 1,2-bis(diphenylmethylene)hydrazine (DPH), tetraphenylethene (TPE), and another unknown compound (X) in the ratio 50/35/15, respectively. The complex **16** also reacted with ^{t}BuPA to obtain cyclo-$(PtBu)_3$ as a major product (Scheme 12) [35].

The reactions between no functional groups on azides and excess alkenes in the presence of **17** (1.0 mol %) at 90 °C for 18 h to obtain aziridines in yields (47−82%). While, the same reaction, but

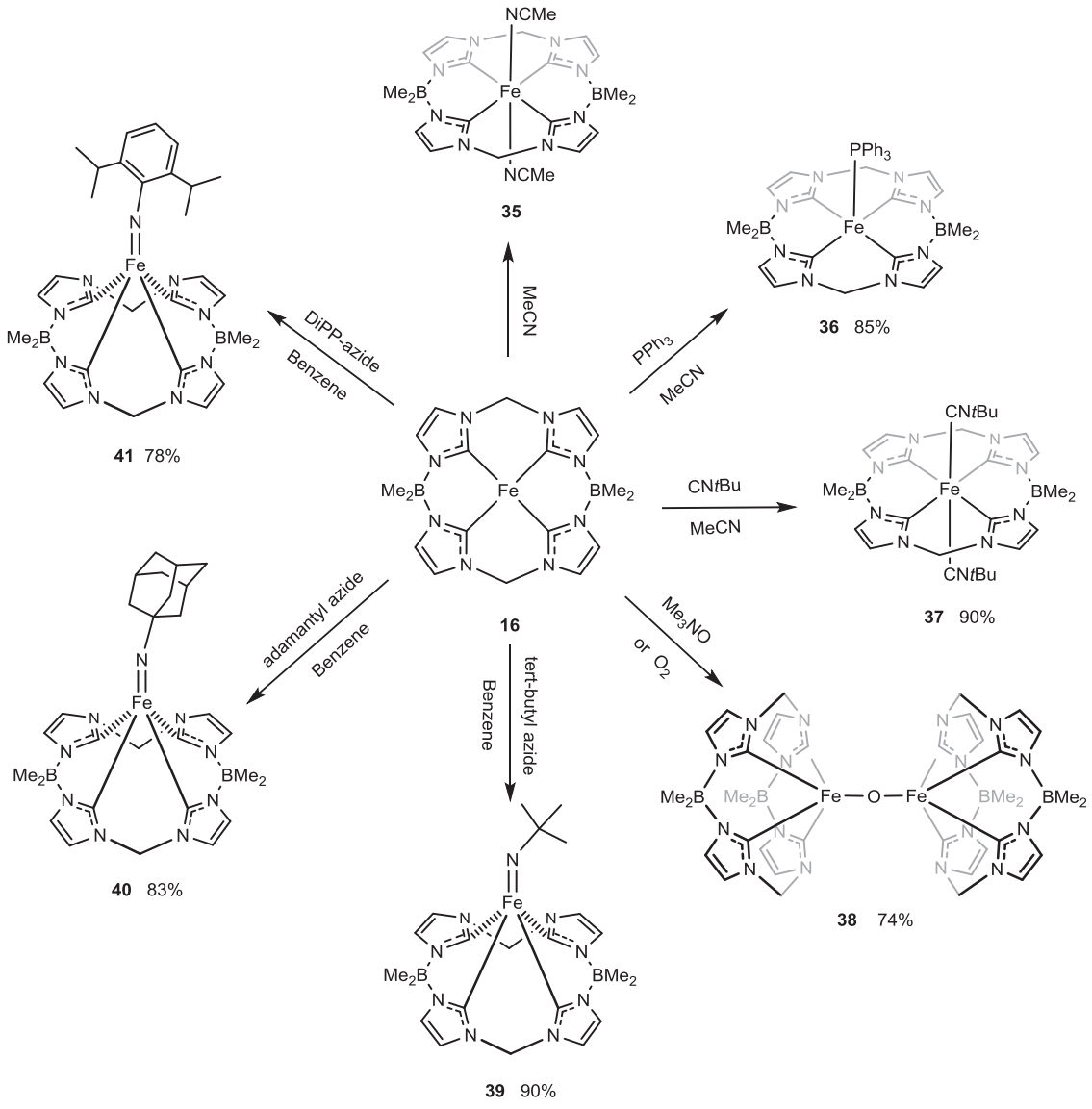

Scheme 10. Reactions of macrocyclic tetra–NHC–Fe complex **16**.

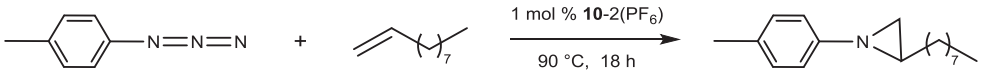

Scheme 11. Aziridination reaction catalyzed by **10**-2(PF_6).

using functional groups on azides with **17** (1.0–10 mol %) obtained aziridines in yields (32–50%). The additional reaction between aryl azides and alkenes with **17** (1.0–5.0 mol %) as the catalyst to obtain aziridines in yields (58–95%) (Scheme 13). The intramolecular aziridination reactions were also tested by using short-chain alkene azides in the presence of **17** (0.1 mol %) to obtain aziridines in yields (30–83%) [43].

Recently, Jenkins and coworkers reported the mechanism of the catalytic aziridination with macrocyclic NHC–Fe^{II} complexes (**10**–2(PF_6) and **17**), azides, and alkenes (Scheme 14) by using DFT and experimentally testing the results. The mechanism included three steps: Firstly, the pathway of an Fe-imide intermediate formed through an α-bound azide and direct loss of N_2. Secondly,

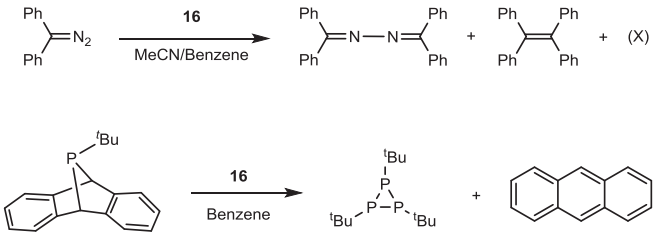

Scheme 12. Reactions of **16** with N_2CPh_2 and ^tBuPA.

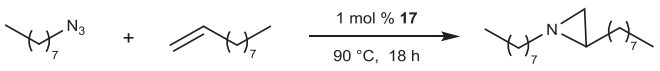

Scheme 13. Aziridination reaction catalyzed by **17**.

the rate determining step of the aziridine formation was the addition of alkene to iron imide. This step favored through a radical pathway (change the stereochemistry), which was proved by DFT calculations and experimental results. Finally, computational and experimental results suggested that using the steric bulk of the organic azide with lower alkene loading in the presence of iron catalysts was more favorer the aziridine formation than the metallotetrazene formation [48].

2.3. Cobalt

In 2009, Murphy and coworkers synthesized the first mononuclear Co^{II} complex **42**−2(I) in low yield (22%) by deprotonation of the macrocyclic imidazolium salt **L**^{7}.4HI using sodium hydride in DMF and then adding anhydrous $CoCl_2$ (Scheme 15) [24]. However, the same complex **42**−2(I)was synthesized by reacting $CoCl_2 \cdot 6H_2O$ with **L**^{7}.4HI in NaOH in good yield 60% (Scheme 15) [24].

The crystal structure of **42-**2(I) had a distorted tetrahedral geometry with Co−C bond distances are around 2.056 Å (Table 3 and Fig. 6). The magnetic moment of this complex (4.9 BM) was consistent with the structure seen in the solid state. For cyclovoltammetric studies, electrochemically active of I^- counterpart was exchanged to BF_4^- counterpart by reacting **42**−2(I)with $AgBF_4$ to obtain **42**−2(BF_4). Cyclic voltammetry for **42**−2(BF_4) showed reversible redox reaction, at potential −1.15 V corresponding to the Co^{II}/Co^{I} (vs. Ag/AgCl/KCl). The NHC−Co^{III} complexes extremely prefer an octahedral geometry, and the authors believed that the NHC ligand conformation was not easy to dissociate and rearrange from tetrahedral to octahedral, therefore there was no oxidation potential corresponding to a Co^{II}/Co^{III} couple seen in the cyclic voltammogram up to 2.0 V [22].

Interestingly, **42**−2(I) used as an electrochemical and chemical catalyst to reduce aryl halides [24]. **42**−2(I) prepared *in situ* and reduced to NHC−Co^{I} complex by sodium amalgam, which affords reduction of aryl halides to form indolines and indoles (Scheme 16). Notably, the major product was indolines, suggesting that **42**−2(I) was not occurred effective interception of alkyl radicals. The yields for reduction of aryl iodides and bromides were high at room temperature, whereas for the aryl chlorides the yields were lower even at elevated temperatures [24]. Electrochemical reduction of aryl iodides in the presence of 1,4-cyclohexadiene and 10 mol % of **42**−2(I), at potential −1.5 V, at room temperature for 18 h, formed indolines in excellent yields (77−95%). The reduction of aryl bromides led to cyclised products in good yield 70% after 24 h at 90 °C, while attempts to reduce aryl chlorides at the same conditions were unsuccessful [24].

The reaction of **1**−4(OTf) and $CoCl_2$ formed the macrocyclic tetra−NHC−Co^{II} complex **43**−OTf in yield 68% (Scheme 17) [33]. In the crystal structure, the Co centre is a square pyramidal geometry, with the triflates ligand in an axial coordination site and four NHC units in equatorial coordination sites (Fig. 6). The Co−C bond distances are in the range 1.907(5)-1.958(5) Å with the average C−Co−C bond angle is 173.6° (Table 3) [33].

2.4. Nickel

2.4.1. Synthesis of nickel tetra-NHC complexes

In 2010, The first macrocyclic tetra−NHC−Ni^{II} **44**−2(I) was synthesized by Murphy and coworkers [25]. The complex was synthesized, in good yield 73%, from reaction of **L**^{7}.4HI with

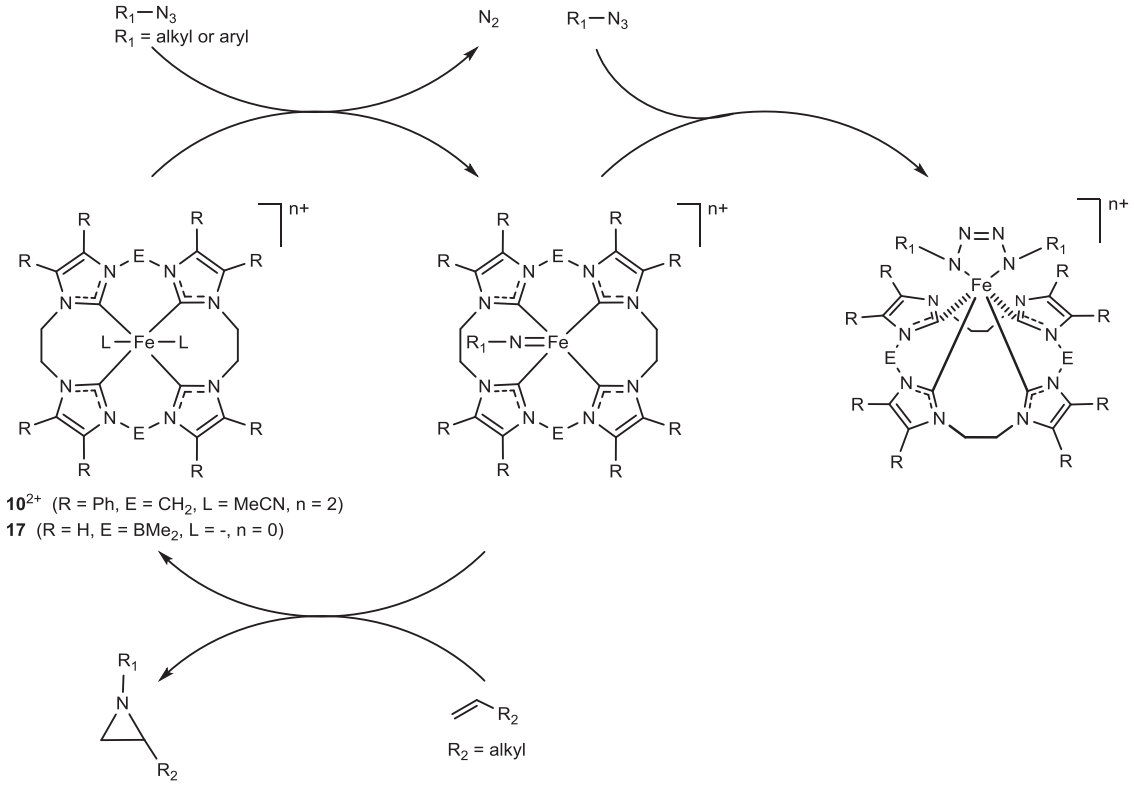

Scheme 14. Proposed mechanism of aziridination from NHC−Fe^{II} complexes **10**$^{2+}$ and **17**.

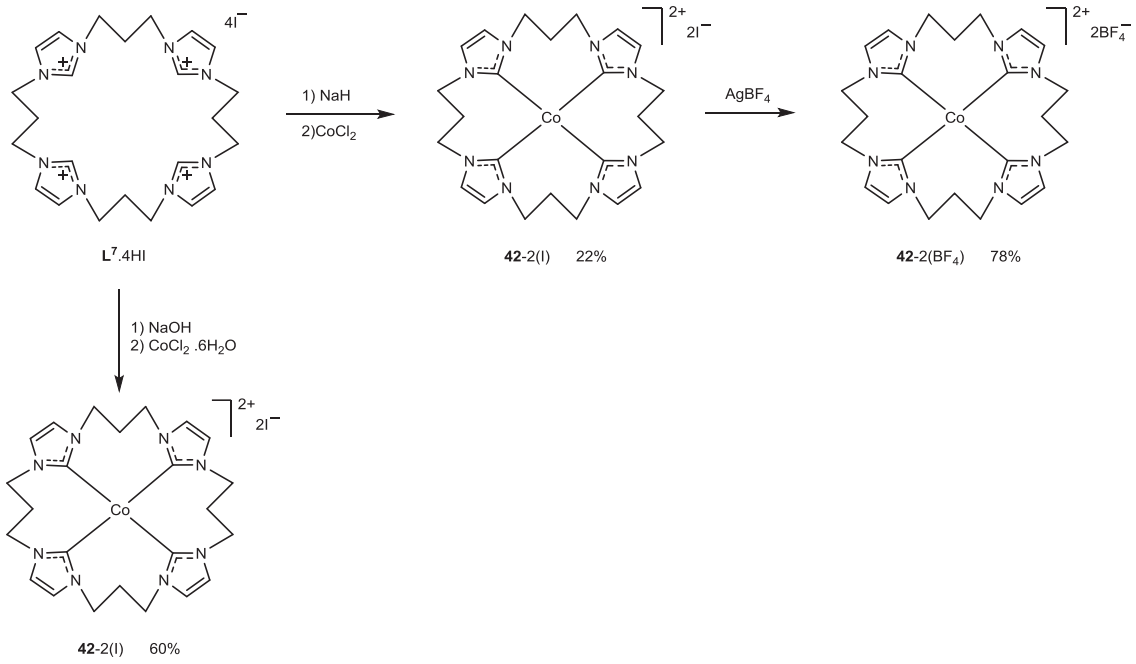

Scheme 15. Synthesis of macrocyclic tetra–NHC–Co^{II} complexes **42**–2(I) and **42**–2(BF_4).

$Ni(OAc)_2$ and NaOAc (Scheme 18) [25]. In the crystal structure, the complex had a square planar geometry with four Ni–C bond distances are 1.900(7) Å (Table 4). The complex **44**–2(I) was reduced to Ni^0 complex **45** by treatment **44**–2(I) with excess Na/Hg in DMF(Scheme 18). Iodide anion of **44**–2(I) was converted into the corresponding PF_6^- anion by metathesis with NH_4PF_6 in methanol was obtained **44**–2(PF_6) in 54% yield (Scheme 18). Cyclovoltammetric studies of **44**–2(PF_6) showed reduction potential at −2.4 V vs Ag/AgCl corresponding to a single electron transfer, and no oxidation potential seen in the CV in the range 0 to +2.5 V. Interestingly, computational studies showed that preventing coordination expansion caused by the conformation of ligand, and the low energy of the filled metal-based orbitals relative to the MOs of the macrocyclic ligand bans the redox process of Ni^{II} [25].

In 2017, a series of mononuclear NHC–Ni^{II} complexes (**46**–2(PF_6) - **49**–2(PF_6)) was synthesized, in similar Murphy's group strategy, by reaction of different macrocyclic ligands with $Ni(OAc)_2$ in the presence of mild base [37,38]. All complexes had a square planar geometry with Ni–C bond distances are in the range 1.900 Å-1.956 Å (Table 4), were characterized by NMR spectroscopy

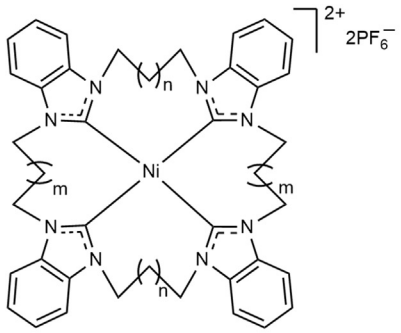

46-2(PF_6), m/n = 1 (57%)
47-2(PF_6), m = 1, n = 2 (65%)
48-2(PF_6), m/n = 2 (54%)

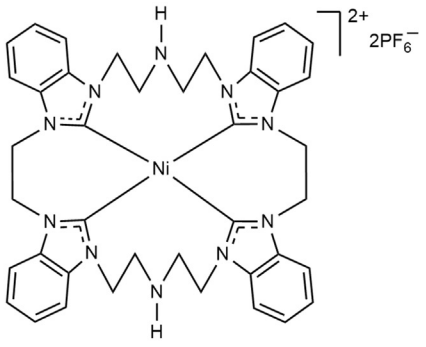

49-2(PF_6) (53%)

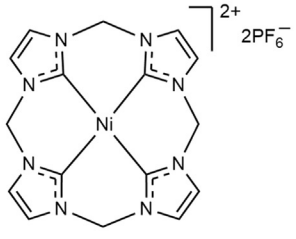

51-2(PF_6) (61%)

Table 3
Selected bond lengths (Å) and angles (°) for Co complexes.

Complexes	L_1	L_2	Co–C	Co-L_1	Co-L_2	C–Co–C	Ref.
42–2(I)	–	–	2.056(4), 2.057(4)	–	–	113.6(2), 111.3(2)	[24]
43–OTf	OTf	–	1.907(5), 1.958(5), 1.913(5), 1.957(5)	2.401(7)	–	169.8(2), 177.3(2)	[33]

and mass spectrometry.

The reaction of $Ni(PPh_3)_2Cl_2$ with **1**–4(OTf) formed macrocyclic tetra–NHC–Ni^{II} complex **50**–2(OTf) in great yield 87% (Scheme 19) [33]. The X-ray studies for **50**–2(OTf) showed a square planar geometry with Ni–C bond distances are in the range 1.870(4)-1.925(4) Å (Table 4) [33]. NHC–Ni^{II} complex **51**–2(PF_6) was

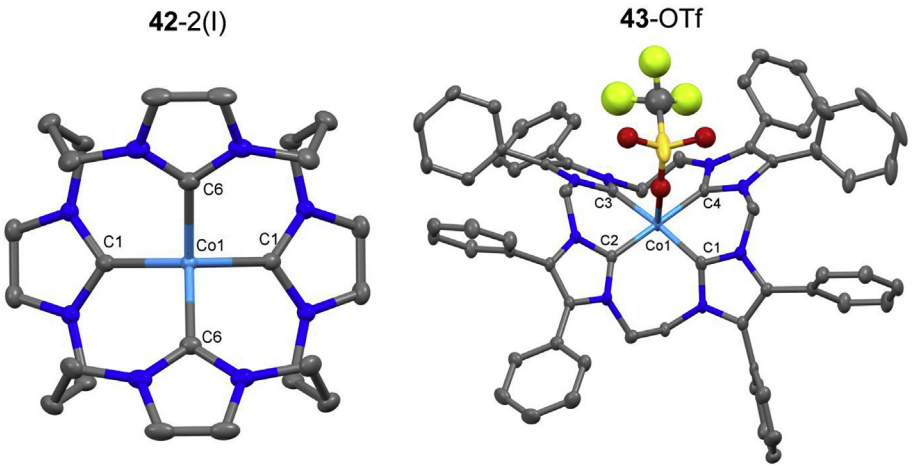

Fig. 6. Crystal structure (50% probability level for the displacement ellipsoids) of the cations of **42**–2(I) and **43**–OTf.

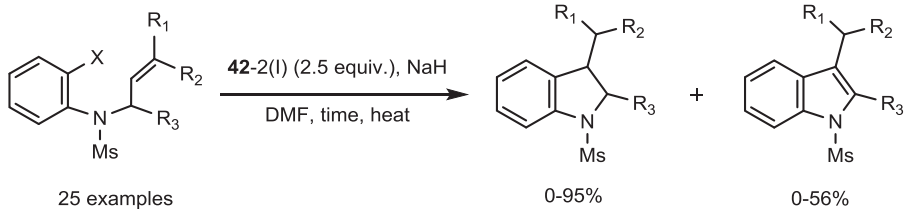

Scheme 16. Reduction of aryl halides catalyzed by **42**–2(I).

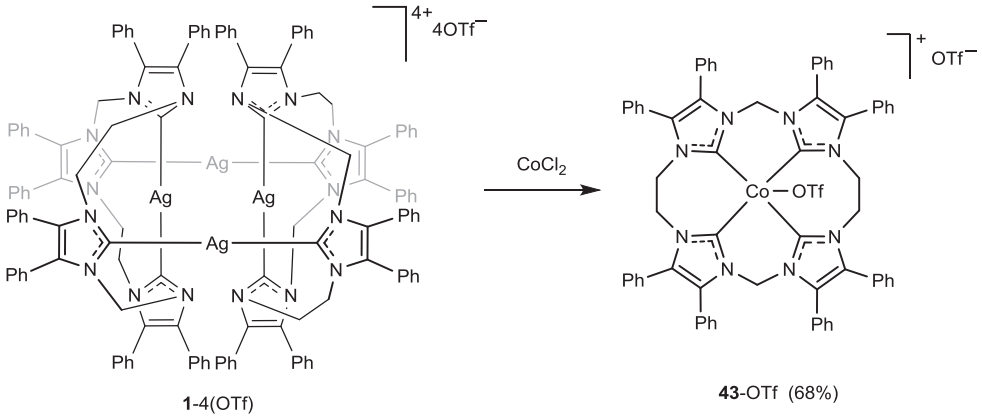

Scheme 17. Synthesis of macrocyclic tetra–NHC–Co^{II} complex **43**–OTf.

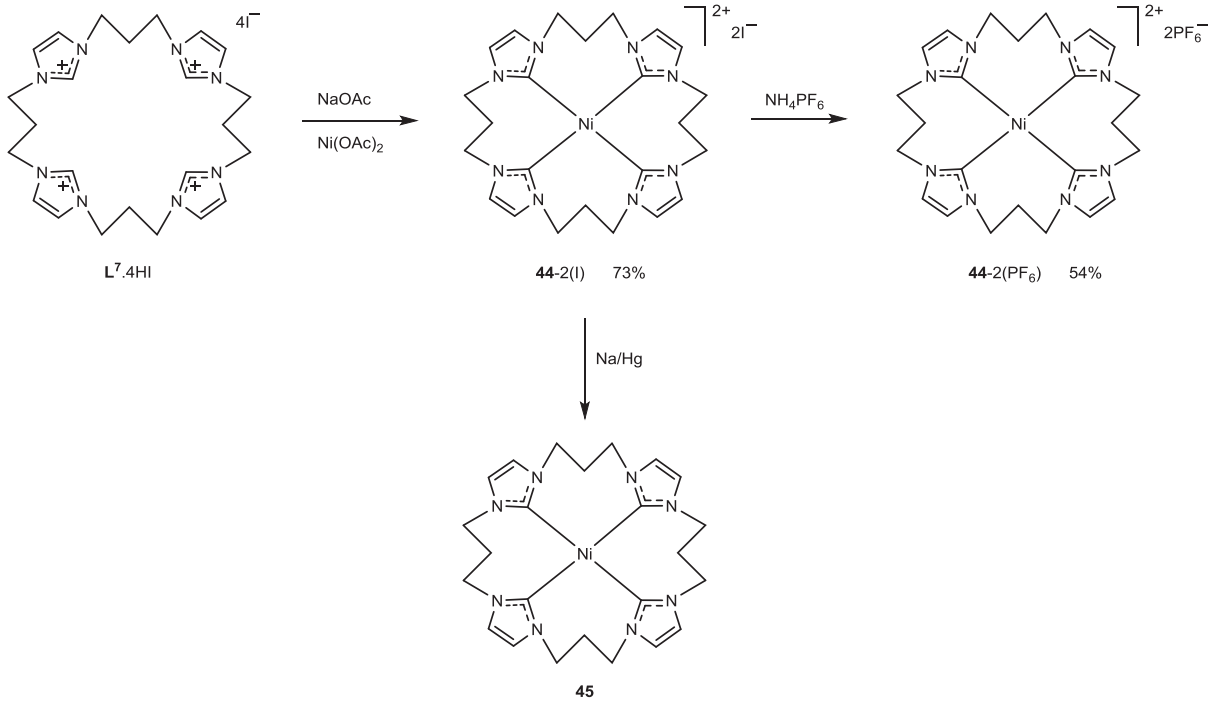

Scheme 18. Synthesis of macrocyclic tetra–NHC–Ni^{II} and -Ni^{0} complexes.

Table 4
Selected bond lengths (Å) and angles (°) for Ni complexes.

Complexes	Ni–C	C–Ni–C	Ref.
44–2(I)	1.900(7)	180	[25]
46–2(PF_6)	1.898(4), 1.902(4), 1.903(4), 1.901(4)	177.7(2), 178.2(2)	[37]
47–2(PF_6)	1.946(6), 1.933(6), 1.956(6), 1.954(6)	172.9(3), 172.4(3)	[37]
48–2(PF_6)	1.954(6), 1.947(7), 1.941(7), 1.899(7)	177.5(3), 176.2(3)	[37]
49–2(PF_6)	1.902(5), 1.905(5)	176.4(3), 171.8(3)	[38]
50–2(OTf)	1.877(4), 1.907(4), 1.870(4), 1.925(4)	174.4(2), 172.1(2)	[33]
51–2(PF_6)	1.851(3), 1.881(3), 1.853(3), 1.886(3)	176.1 (1), 175.4 (1)	[49]
53	1.927(3), 1.891(3)	172.0(2), 175.8(2)	[50]

synthesized by a similar strategy in yield 61% [49]. In the crystal structure, the complex had also a square planar geometry with Ni–C bond distances are in the range 1.851(3)-1.886(3) Å (Table 4). The complex was characterized by NMR spectroscopy and mass spectrometry.

Attempts to synthesize **52** from 16-atom macrocyclic imidazolium diborate slat $\mathbf{L^8}$.2HI was unsuccessful. However, the reaction of 18-atom macrocyclic $\mathbf{L^1}$.2HBr with nBuLi and NiI_2 obtained **53** in low yield 10% (Scheme 20). The main reason for the unsuccessful synthesis of **52** was the inability to deprotonate the imidazolium salts because of having high electron-donation of the imidazolium salts. The complex **53** had a square planar geometry (Table 4 and Fig. 7). The complex **53** was also characterized by HR-DART/MS and NMR [50].

2.4.2. Catalytic applications of nickel tetra-NHC complexes

The Birch reduction of substituted anthracenes in the presence of **45** worked successfully with yields (54–85%) (Scheme 21). The complex **45** also reacted with carbonyl compounds to obtain (*d*,*L*)-isomer of the corresponding products of the pinacol reaction in

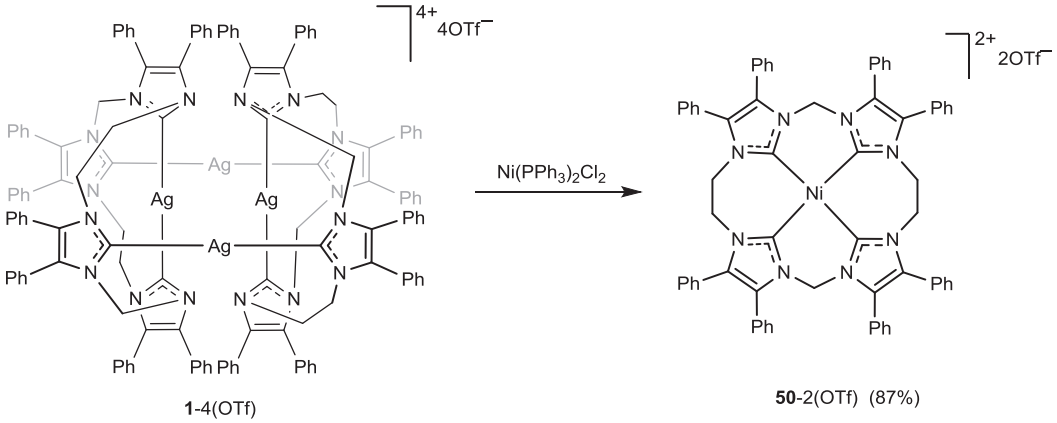

Scheme 19. Synthesis of macrocyclic tetra–NHC–Ni^{II} complex **50**–2(OTf).

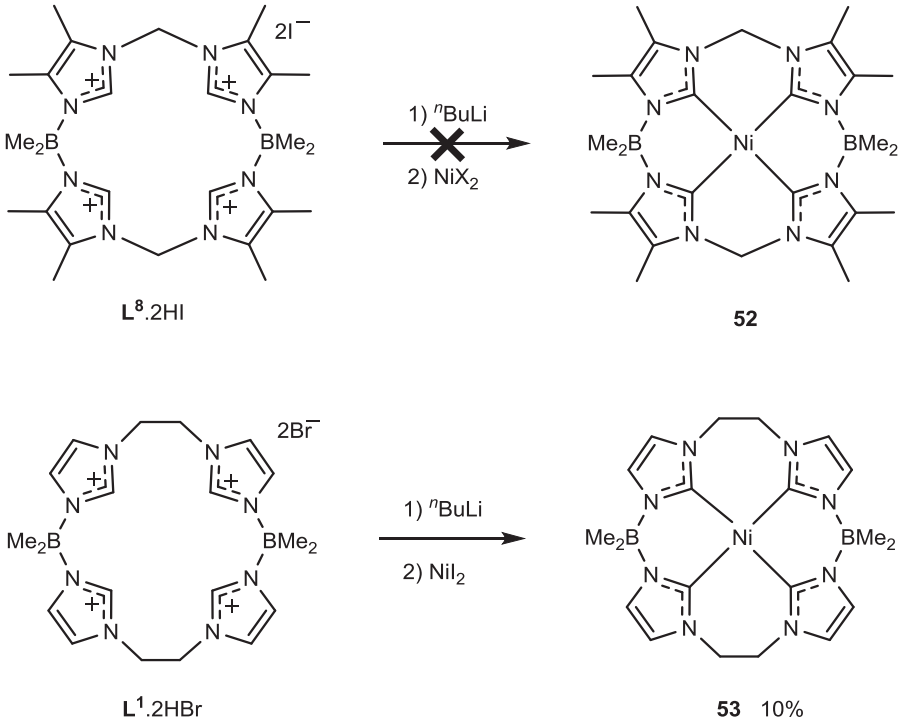

Scheme 20. Synthesis of macrocyclic tetra–NHC–Ni^{II} complex **53**.

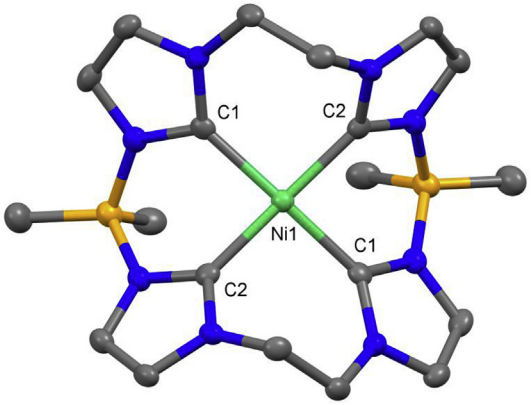

Fig. 7. Crystal structure (50% probability level for the displacement ellipsoids) of **53**.

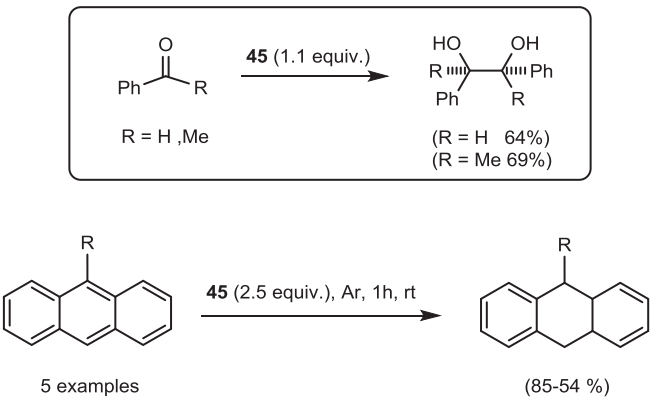

Scheme 21. Reductions of carbonyl compounds and of substituted anthracenes catalyzed by **45**.

yields (64–69%), and reduced *p*-toluenesulfonamides in yields (72–99%). Finally, The reduction of *cis*- and *trans*-stilbene oxides was occurred by **45** with low to good yields (18–71%) [25].

2.5. Copper

The first macrocyclic tetracarbene Cu^{III} complex was synthesized by direct complexation between $\mathbf{L^5}.4HPF_6$ and Cu^{II} acetate at 40 °C in high yield 90% (Scheme 22) [51].

The crystal structure had a square planar geometry with four Cu^{III}–C bond distances are in the range 1.879(5)-1.883(5) Å, which is shorter than for Cu^{I}–C bonds (1.90–1.95 Å) and Cu^{II}–C bonds (1.89–1.99 Å) (Fig. 8) [51]. Cyclovoltammetric studies exhibited that the **54**–$3(PF_6)$ showed an irreversible reduction at −1.14 V and partially reversible reduction at −0.75 V, as well as the irreversible oxidation at +1.69 V in acetonitrile [51].

2.6. Rhodium and Ruthenium

The transmetalation reaction of **1**–$4(PF_6)$ and RhI_3 obtained the macrocyclic tetra–NHC–Rh^{III} complex **55**–PF_6 in good yield 72%. The macrocyclic tetra–NHC–Ru^{II} complex **56**–2(OTf) was formed, in low yield 40%, by using $Ru(DMSO)_4Cl_2$ with **1**–4(OTf) [33]. The crystal structure of **55**–PF_6 showed two iodide ligands in axial coordination sites. The solid state of **56**–2(OTf) was octahedral geometry having two solvent ligands (DMSO) in axial coordination sites (Fig. 9), with the average Ru–C bond distance is 2.107 Å. The structure of **56**–2(OTf) was also confirmed by NMR spectroscopy and mass spectrometry.

2.7. Palladium

In 2007, Murphy et al. synthesized the first macrocyclic

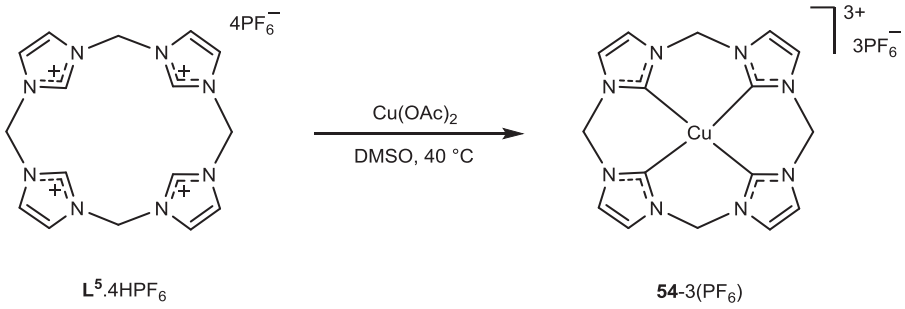

Scheme 22. Synthesis of macrocyclic tetra−NHC−Cu^{III} complex **54**−3(PF_6).

tetra−NHC−Pd^{II} **57**−2(I), in good yield 87%, by reaction of **L**[7].4HI with PdI_2 in the presence of a mild base (Scheme 23). Crystal structure for **57**−2(I) had a square planar geometry with Pd−C bond distances are about 2.03 Å. The complex **57**−2(I) was characterized by infrared and NMR spectroscopy and mass spectrometry [23].

The transmetalation reaction of **1**−4(OTf) and PdI_2 formed **58**−2(OTf) in yield 70% [33]. A similar strategy was reported to the synthesis of **59**-2(PF_6) in yield 68% by using $PdCl_2(PPh_3)_2$ source [49]. The crystal structures for **58**−2(OTf) and **59**−2(PF_6) had a square planar geometry with the Pd−C bond distances are in the range 1.987(7)- 2.041(6) Å (Table 5) [33,49].

Similar to the synthesis of **53**, 18-atom macrocyclic tetra−NHC−Pd^{II} complex (**60**) was also obtained in low yield 9%. The crystal structure of the complex was a square planer with Pd−C bond lengths are in the range 2.015(2)- 2.057(2) Å (Table 5 and Fig. 10 (A)) [50].

In 2017, some mononuclear Pd^{II} complexes (**61**−2(PF_6) - **64**−2(PF_6)) was synthesized by reaction of different macrocyclic ligands with $Pd(OAc)_2$ in the presence of NaOAc. All complexes had also a square planar geometry with Pd−C bond distances are in the range 2.025−2.072 Å (Table 5 and Fig. 10 (B)) [37,38], which are slightly longer than Pd−C bond distances seen in the other macrocyclic NHC−Pd^{II} complexes [33,49,50]. These complexes were also characterized by NMR spectroscopy and mass spectrometry [37,38].

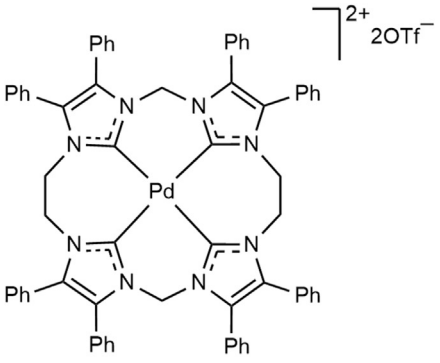

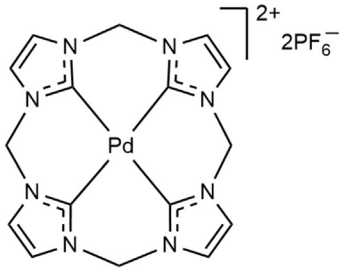

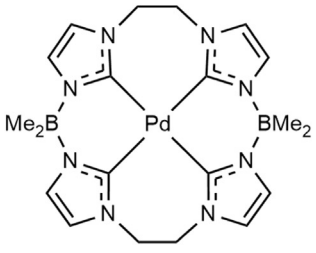

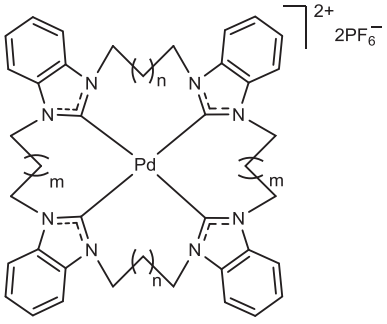

61-2(PF_6), m/n = 1 (47 %)
62-2(PF_6), m = 1, n = 2 (42%)
63-2(PF_6), m/n = 2 (43%)

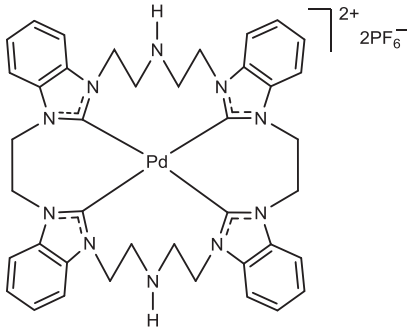

64-2(PF_6) (45%)

2.8. Platinum

In 2005, the first macrocyclic tetra–NHC–Pt^{II} complex **66**–2(Cl) was reported by Hahn and coworkers [21]. The complex **66**–2(Cl) was synthesized, in moderate yield, by the treatment of **65**–2(CF_3SO_3) with diphosgene in DMF (Scheme 24) [21,22].

The X-ray studies for **66**–2(Cl) showed a square planner geometry with Pt–C bond distances are in the range 1.969(4)-1.980(4) Å (Table 6 and Fig. 11) [21].

Complexes **67**–2(OTf) and **68**–2(PF_6) were synthesized, in low yield 46% and 7%, respectively, by reaction of imidazolium salts (**L^3**.4HOTf and **L^2**.4HI) with platinum salt sources in the presence of weak base (Scheme 25). Both complexes were characterized by NMR spectroscopy and mass spectrometry [52].

The transmetalation reaction of **1**–4(OTf) and $PtCl_2(NCPh)_2$ obtained **68**–2(OTf) in high yield 93% (Scheme 25) [33]. Besides, **69**–2(PF_6) was synthesized, in yield 65%, with a similar strategy of **68**–2(OTf) synthesis [49]. Complexes **68**–2(OTf) and **69**–2(PF_6) had a square planer geometry with Pt–C bond lengths are in the range 1.995(8) –2.035(7) Å (Table 6) [33,49].

In 2017, a series of mononuclear Pt^{II} complexes (**70**–2(PF_6) **-72**–2(PF_6)) was obtained by reaction of different macrocyclic ligands with $Pt(acac)_2$ in the presence of mild base [37]. All complexes had also a square planar geometry with Pt–C bond distances are in the range 2.019–2.081 Å (Table 6) [37], which are consistent with other macrocyclic tetra-NHC Pt^{II} complexes [21,33,49,52].

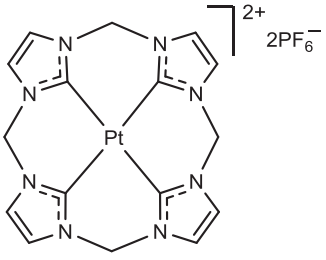

69-2(PF_6) (65%)

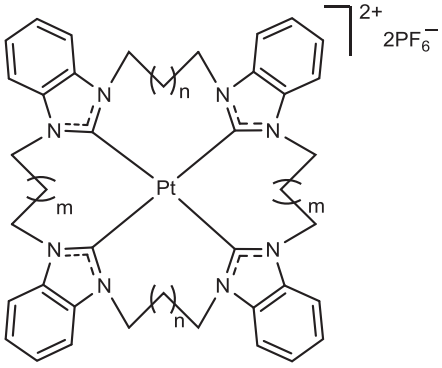

70-2(PF_6), m/n = 1 (60 %)
71-2(PF_6), m = 1, n = 2 (57%)
72-2(PF_6), m/n = 2 (55%)

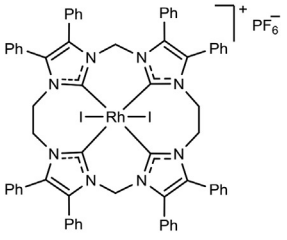

55-PF_6 (72%)

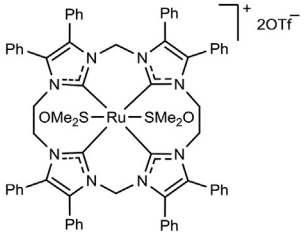

56-2(OTf) (40%)

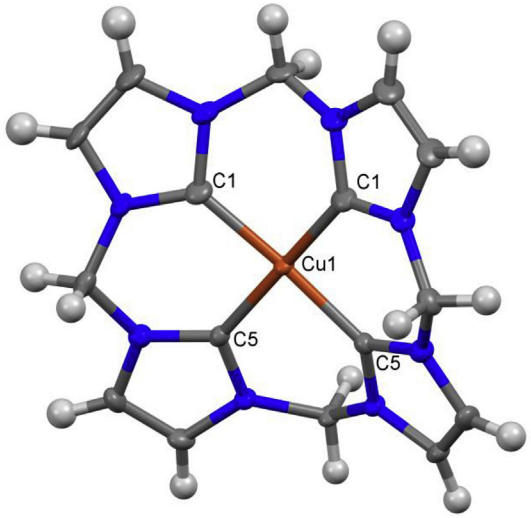

Fig. 8. Crystal structure (50% probability level for the displacement ellipsoids) of the cation of **54**–3(PF_6).

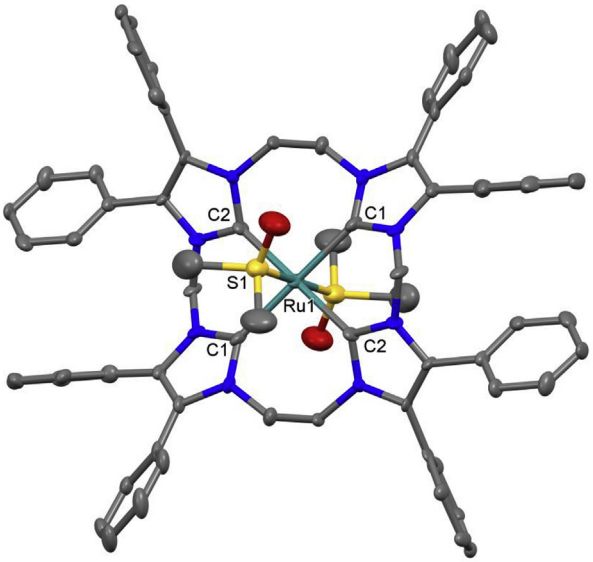

Fig. 9. Crystal structure (30% probability level for the displacement ellipsoids) of the cation of **56**–2(OTf).

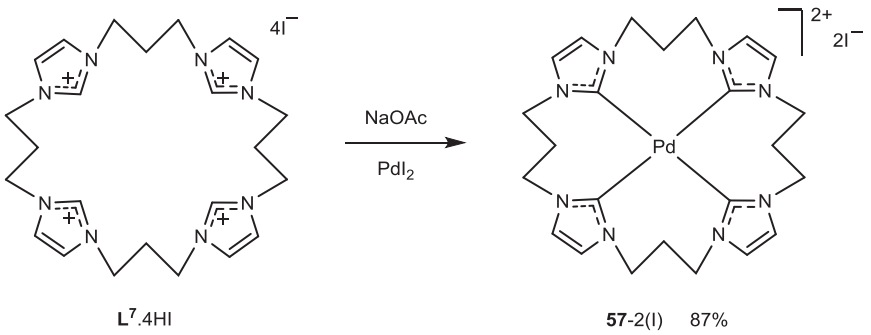

Scheme 23. Synthesis of macrocyclic tetra–NHC–Pd^{II} complex **57**–2(I).

Table 5
Selected bond lengths (Å) and angles (°) for Pd complexes.

Complexes	Pd–C	C–Pd–C	Ref
58–2(OTf)	2.037(6), 1.999(7), 2.041(6), 1.988(7)	172.4(3), 179.7(3)	[33]
59–2(PF_6)	1.987(2), 1.987(2), 1.992(2), 1.992(2)	172.85(9), 172.85(9)	[49]
60	2.015(2), 2.057(2)	174.4(1), 174.8(1)	[50]
61–2(PF_6)	2.044(4), 2.033(5), 2.042(4), 2.025(5)	178.7(2), 176.3(2)	[37]
62–2(PF_6)	2.036(9), 2.056(9), 2.056(8), 2.045(9)	175.6(4), 176.4(4)	[37]
63–2(PF_6)	2.100(10), 2.029(9), 2.051(9), 2.039(9)	178.5(4), 177.5(3)	[37]
64–2(PF_6)	2.049(3), 2.055(4)	171.35(18)	[38]

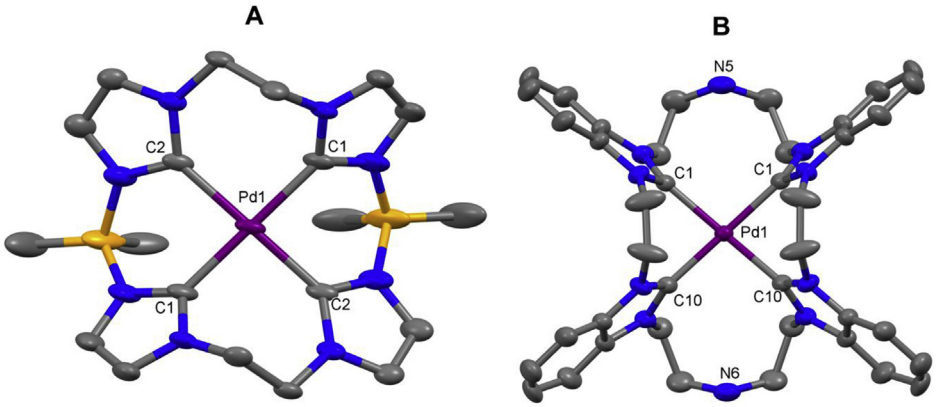

Fig. 10. (A) Crystal structure (50% probability level for the displacement ellipsoids) of **60**. **(B)** Crystal structure (30% probability level for the displacement ellipsoids) of the cation of **64**–2(PF_6).

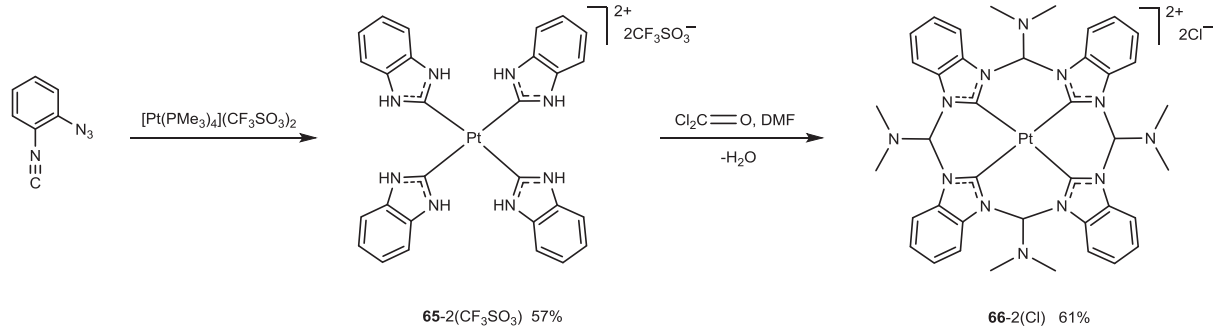

Scheme 24. The first synthesis of macrocyclic tetra–NHC–Pt^{II} complex **66**–2(Cl).

2.9. Gold

The first macrocyclic tetra–NHC–Au^{III} complex **73**–3(OTf) was reported by Jenkins and coworkers in 2012. The transmetalation reaction of **1**–4(OTf) and $HAuCl_4$ obtained **73**–3(OTf) in low yield 47%. The complex **73**–3(OTf) had a square planar geometry with

Table 6
Selected bond lengths (Å) and angles (°) for Pt complexes.

Complexes	Pt–C	C–Pt–C	Ref.
66–2(Cl)	1.980(4), 1.969(4), 1.973(4), 1.978(4)	179.03(15), 178.77(15)	[21]
68–2(PF_6)	2.04(2), 2.10(1), 1.94(2), 1.97(1)	173.4(6), 174.6(6)	[52]
68–2(OTf)	2.025(8), 1.995(8), 2.035(7), 1.996(8)	173.7(3), 179.6(4)	[33]
69–2(PF_6)	1.970(7), 1.981(7), 1.983(8), 1.994(7)	175.1(3), 175.9(3)	[49]
70–2(PF_6)	2.017(9), 2.036(10), 2.019(8), 2.041(10)	178.9(4), 176.3(4)	[37]
71–2(PF_6)	2.050(5), 2.035(5), 2.041(5), 2.034(5)	176.6(2), 177.3(2)	[37]
72–2(PF_6)	2.060(9), 2.081(10), 2.061(9), 2.075(10)	177.9(4), 177.7(4)	[37]

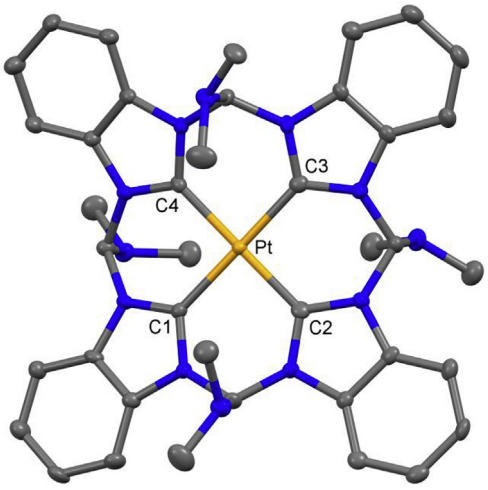

Fig. 11. Crystal structure (50% probability level for the displacement ellipsoids) of the cation of **66**–2(Cl).

Au–C bond distances are in the range 2.017(9)- 2.052(9) Å (Fig. 12) [33].

Recently, Baker group was also synthesized macrocyclic tetra-NHC Au^{III} complexes (**74**–Cl and **75**–3(PF_6)) by heating $KAuCl_4$ with the macrocyclic imidazolium salt $\mathbf{L^8}$.4HCl in the presence of base to obtain Au^{III}–NHC chlorido **74**–Cl, and treated **74**–Cl with KPF_6 to give four-coordinate Au^{III} complex **75**–3(PF_6) (Scheme 26) [53]. The X-ray studies for **74**–Cl and **75**–3(PF_6) showed that NHC groups shaped approximate square planar around the Au atom. Au–C bond distances are in the range 2.048(8)-2.082(7) Å (Table 7). In **74**–Cl, two Cl^- ligands occupy the apical position, Au–Cl bond distance being about 3.016(4) Å, so that the complex showed distorted octahedral geometry. NMR studies and conductance measurements for **74**–Cl and **75**–3(PF_6) in DMSO solution were consistent with the structures seen in the solid state [53]. Cyclovoltammetric studies of **74**–Cl showed two reduction potentials, at - 0.09 (Au^{III}/Au^{I}) and - 0.78 V (Au^{I}/Au^{0}), and three oxidation potentials, at - 0.56 (Au^{0}/Au^{I}), +0.71 and + 1.12 V (Cl^-/0.5 Cl_2 and Au^{0}/Au^{I} deposited on the electrode) [53–55]. In **75**–3(PF_6), the processes showed similar potentials as seen for chlorido complex,

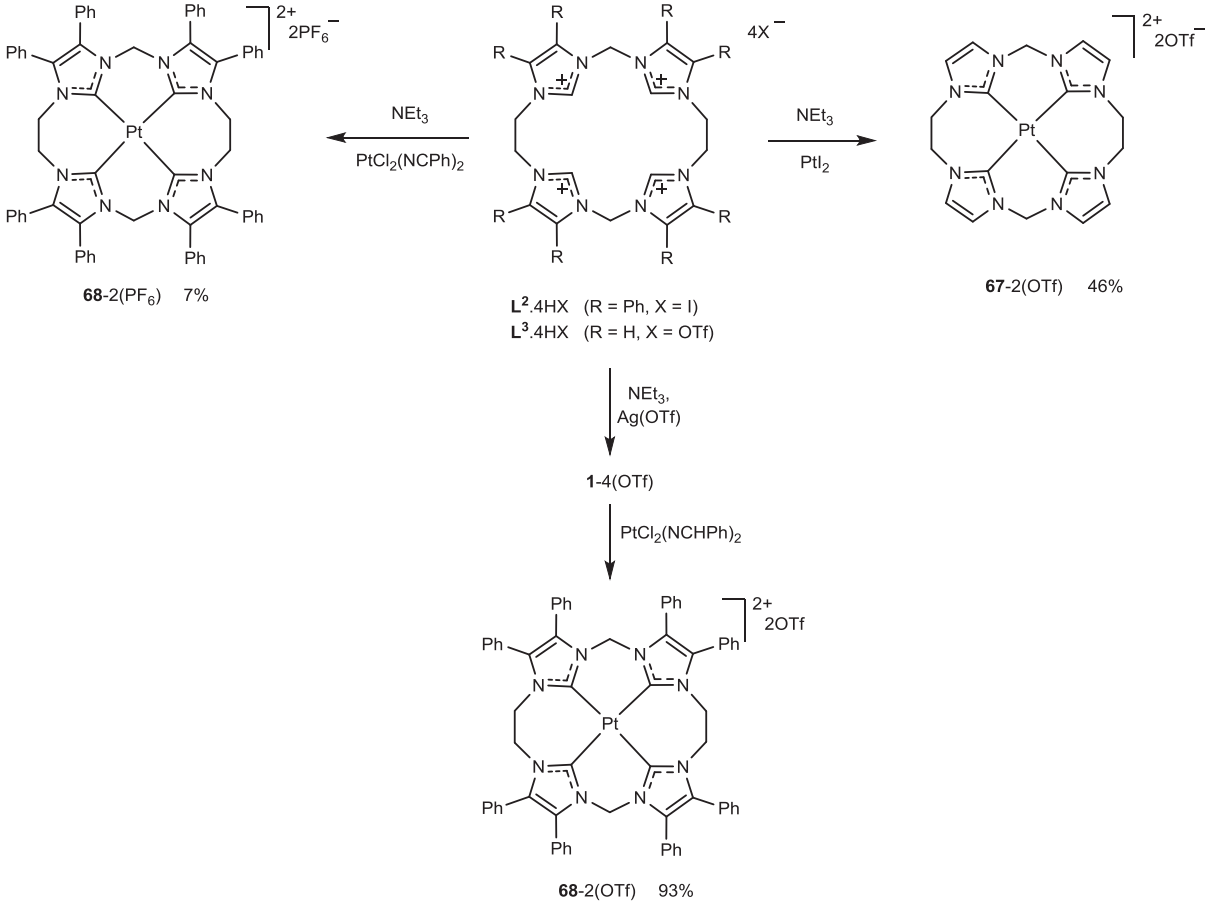

Scheme 25. Synthesis of macrocyclic tetra–NHC–Pt^{II} complexes **67**–2(OTf) and **68**–2(OTf).

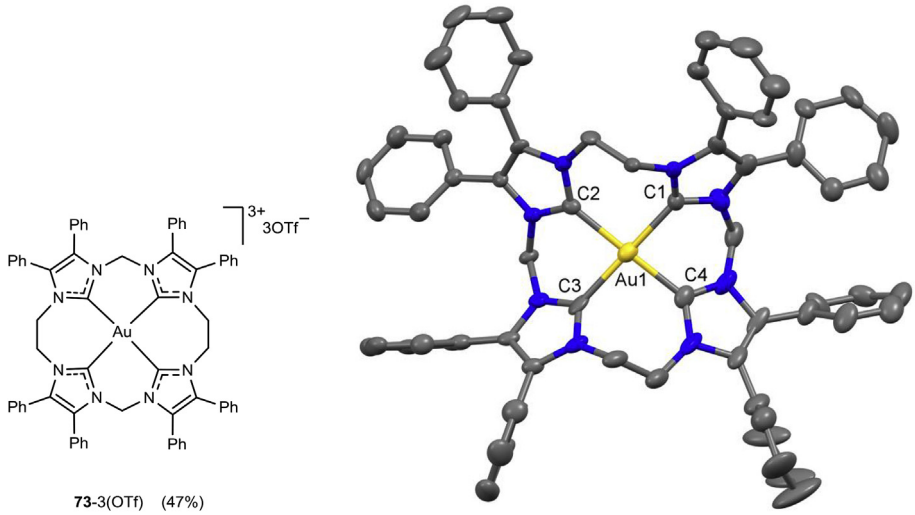

Fig. 12. Crystal structure (50% probability level for the displacement ellipsoids) of the cation of **73**.3(OTf).

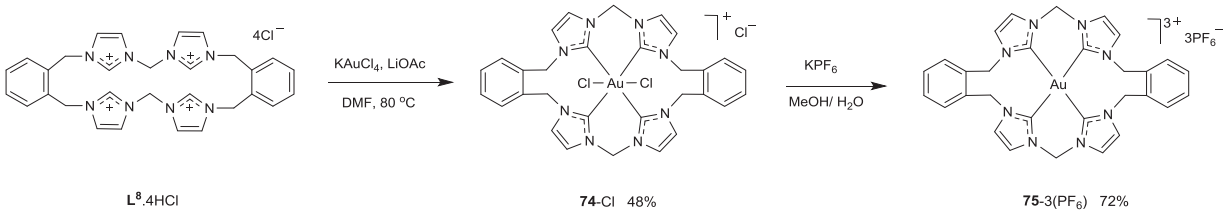

Scheme 26. Synthesis of macrocyclic tetra–NHC–Au^{III} complexes **74**–Cl and **75**–3(PF_6).

Table 7
Selected bond lengths (Å) and angles (°) for Au complexes.

Complexes	$L_{1/2}$	Au–C	Au-$L_{1/2}$	C–Au–C	Ref.
73–3(OTf)	–	2.017(9), 2.052(9), 2.030(11), 2.042(10)	–	174.5(4), 174.5(4)	[33]
74–Cl	Cl	2.048(8), 2.082(7)	3.016(4)	180	[53]
75–3(PF_6)	–	2.050(2), 2.055(2)	–	180	[53]

excluding oxidation potential for (Cl^-/0.5 Cl_2) [53].

2.10. Tin, Indium, and Aluminium

Attempts to synthesize a group 13 or 14 metal complex from **L^2**.4HOTf was unsuccessful. However, the reaction of **L^1**.2HBr with ^{n}BuLi and MBr_n (M = Sn, In and Al) obtained the first three complexes **76**, **77** and **78** in low yield (Scheme 27) [56]. All complexes are air sensitive in solid state and solution. In the crystal structure of **76**, there were two molecules in the unit cell, each of them had an octahedral geometry with two bromide ligands in axial coordination sites. In molecule 1, there was notable bending of one of the bromide ligands due to the steric repulsion between the bromide ligands and the borate methyl groups (Fig. 13). The crystal structure of **77** had a distorted square pyramidal geometry with one bromide ligand in axial coordination site. **78** was modified by substituting chloride for bromide ligand. Its structure had also a distorted square pyramidal geometry with one chloride ligand in axial coordination site (Table 8). All complexes were also characterized by NMR spectroscopy and mass spectrometry. The ^{1}H NMR spectrum of **76** in solution showed that the complex was fluxional behaviour, while complexes **77** and **78** were rigid on the NMR timescale. Therefore, all complexes in solution were consistent with the structures seen in the solid state [56].

3. Conclusions

The expansion of the macrocyclic NHC ligands and their complexes in the last decade presented unique structural and reactivity properties and led to the appearance of interesting catalytic applications. Based on this expansion, the scope is predicted to grow further shortly.

The silver complex has been used in the synthesis of a difference of mononuclear tetra-NHC metal complexes in moderate to high yield by transmetallation reaction. While the most tetra-NHC metal complexes were synthesized by direct complexation between the macrocyclic NHC ligands and metal sources. Interestingly, the new synthetic protocol has been reported for the synthesis of macrocyclic tetra–NHC–Au^{III} and -Cu^{III} complexes in good yield. Notably, the synthesis of tetra–NHC–Ni^{II} and -Pd^{II} complexes from 16-atom macrocyclic tetraimidazolium diborate ligand was unsuccessful. The synthesis of complexes of group 13 and 14 metals from 18-atom macrocyclic tetraimidazolium ligand was also unsuccessful.

The catalytic application of the macrocyclic tetra–NHC–metal complexes is emerging as a remarkable area of research. The macrocyclic tetra–NHC–Cr^{III}, -Fe^{II}, and -Ni^{II} complexes have been used as catalysts for interesting organic synthesis. The first example of aziridination catalysis with the macrocyclic tetra–NHC–Cr^{III} has been reported and obtained C2 + N1 aziridination in low yields. Interestingly, the macrocyclic tetra–NHC–Fe^{II} complex has been successfully used for the catalytic aziridination of olefins. The macrocyclic tetra–NHC–Ni^0 complex has been well utilized in the Birch reduction of substituted anthracenes as well as reduction of

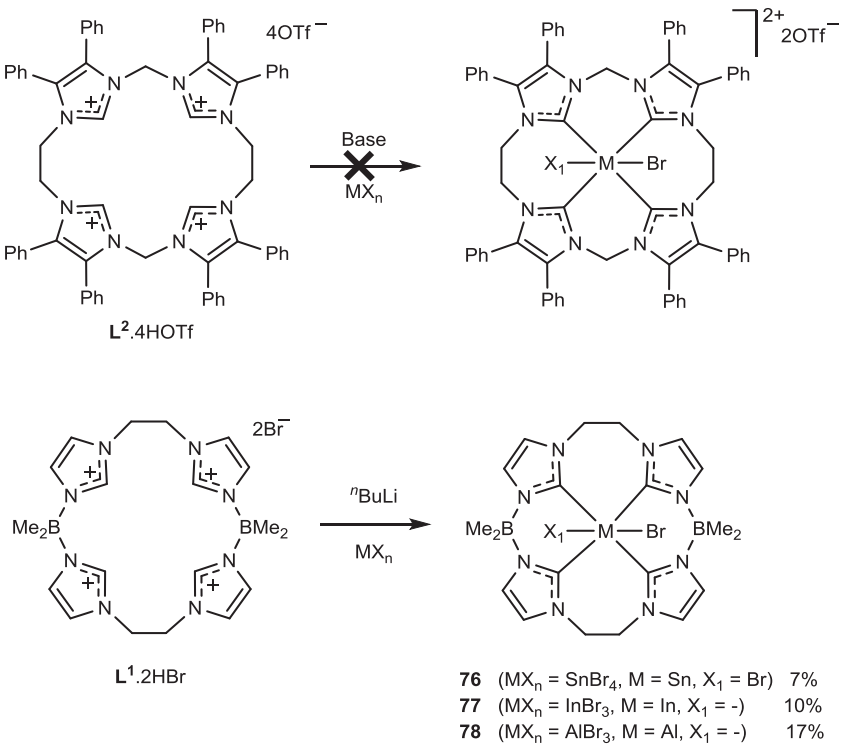

Scheme 27. Synthesis of macrocyclic tetra–NHC–metal complexes (**76**–**78**).

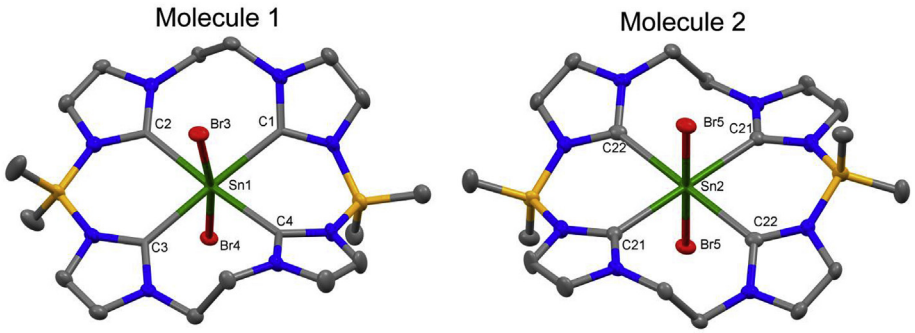

Fig. 13. Crystal structure (50% probability level for the displacement ellipsoids) of **76**.

Table 8
Selected bond lengths (Å) and angles (°) for **76**–**78**.

Complexes	M	L_1	L_2	M-C	M-L_1	M-L_2	C-M-C	L_1-M-L_2	Ref.
76[a]	Sn	Br	Br	2.295(4), 2.276(4), 2.284(5), 2.282(4) *2.307(4), 2.293(4)*	2.6643(5) *2.6074(5)*	2.6255(5) *2.6074(5)*	176.2(2), 175.9(2) *180.0*	172.11(2), *180.0*	[56]
77	In	Br	–	2.28(1), 2.22(1), 2.28(1), 2.23(1);	1.594(2)	–	151.7(4), 173.7(4)	–	[56]
78	Al	Cl	–	2.130(5), 2.080(5)	2.275(3)	–	146.1(3), 165.1(3)	–	[56]

[a] Normal font for molecule 1; *Italics* font for molecule 2.

carbonyl compounds.

The macrocyclic tetra−NHC−Fe complexes with their catalytic applications are widely becoming popular. However, other transition metal complexes (especially Ru, Rh, and Ir) are still rare, which need more investigation. Due to these complexes have promising applications, it can be expected to synthesis new macrocyclic tetra-NHC ligands and their metal complexes in the future.

Acknowledgements

The author acknowledges the Ministry of Higher Education and Scientific Research in Iraq for financial support.

References

[1] K. Öfele, J. Organomet. Chem. 12 (1968) 42−43.
[2] H.W. Wanzlick, H.J. Schönherr, Angew. Chem. Int. Ed. 7 (1968) 141−142.
[3] A. Kascatan-Nebioglu, M.J. Panzner, C.A. Tessier, C.L. Cannon, W.J. Youngs, Coord. Chem. Rev. 251 (2007) 884−895.
[4] J.C. Garrison, W.J. Youngs, Chem. Rev. 105 (2005) 3978−4008.
[5] J.C. Lin, R.T. Huang, C.S. Lee, A. Bhattacharyya, W.S. Hwang, I.J. Lin, Chem. Rev. 109 (2009) 3561−3598.
[6] O. Kühl, Chem. Soc. Rev. 36 (2007) 592−607.
[7] K.M. Hindi, M.J. Panzner, C.A. Tessier, C.L. Cannon, W.J. Youngs, Chem. Rev. 109 (2009) 3859−3884.
[8] V. Charra, P. de Fremont, P. Braunstein, Coord. Chem. Rev. 341 (2017) 53−176.
[9] A.A. Danopoulos, T. Simler, P. Braunstein, Chem. Rev. 119 (6) (2019) 3730−3961.
[10] S. Bellemin-Laponnaz, S. Dagorne, Chem. Rev. 114 (2014) 8747−8774.
[11] M.-M. Gan, J.-Q. Liu, L. Zhang, Y.-Y. Wang, F.E. Hahn, Y.-F. Han, Chem. Rev. 118 (2018) 9587−9641.
[12] K. Riener, S. Haslinger, A. Raba, M.P. Högerl, M. Cokoja, W.A. Herrmann, F.E. Kühn, Chem. Rev. 114 (2014) 5215−5272.
[13] F.E. Hahn, ChemCatChem 5 (2013) 419−430.
[14] Z. Wang, L. Jiang, D.K.B. Mohamed, J. Zhao, T.A. Hor, Coord. Chem. Rev. 293 (2015) 292−326.
[15] A. Prakasham, P. Ghosh, Inorg. Chim. Acta 431 (2015) 61−100.
[16] M. Mora, M.C. Gimeno, R. Visbal, Chem. Soc. Rev. 48 (2019) 447−462.
[17] M.N. Hopkinson, C. Richter, M. Schedler, F. Glorius, Nature 510 (2014) 485−496.
[18] W. Zhao, V. Ferro, M.V. Baker, Coord. Chem. Rev. 339 (2017) 1−16.
[19] M.V. Baker, B.W. Skelton, A.H. White, C.C. Williams, J. Chem. Soc., Dalton Trans. (2001) 111−120.
[20] G. Lovat, E.A. Doud, D. Lu, G. Kladnik, M.S. Inkpen, M.L. Steigerwald, D. Cvetko, M.S. Hybertsen, A. Morgante, X. Roy, Chem. Sci. 10 (2019) 930−935.
[21] F.E. Hahn, V. Langenhahn, T. Lügger, T. Pape, D. Le Van, Angew. Chem. Int. Ed. 44 (2005) 3759−3763.
[22] P.G. Edwards, F.E. Hahn, Dalton Trans. 40 (2011) 10278−10288.
[23] R. McKie, J.A. Murphy, S.R. Park, M.D. Spicer, S.z. Zhou, Angew. Chem. Int. Ed. 46 (2007) 6525−6528.
[24] S.R. Park, N.J. Findlay, J. Garnier, S. Zhou, M.D. Spicer, J.A. Murphy, Tetrahedron 65 (2009) 10756−10761.
[25] N.J. Findlay, S.R. Park, F. Schoenebeck, E. Cahard, S.-z. Zhou, L.E. Berlouis, M.D. Spicer, T. Tuttle, J.A. Murphy, J. Am. Chem. Soc. 132 (2010) 15462−15464.
[26] A.J. Birch, J. Chem. Soc. (1944) 430−436.
[27] P.W. Rabideau, E.G. Burkholder, J. Org. Chem. 43 (1978) 4283−4288.
[28] P.W. Rabideau, Tetrahedron 45 (1989) 1579−1603.
[29] T. Ankner, G. Hilmersson, Tetrahedron 65 (2009) 10856−10862.
[30] Y. Kashiwagi, C. Kikuchi, F. Kurashima, J.-i. Anzai, J. Organomet. Chem. 662 (2002) 9−13.
[31] G. Radivoy, F. Alonso, M. Yus, Tetrahedron 55 (1999) 14479−14490.
[32] S.A. Cramer, D.M. Jenkins, J. Am. Chem. Soc. 133 (2011) 19342−19345.
[33] Z. Lu, S.A. Cramer, D.M. Jenkins, Chem. Sci. 3 (2012) 3081−3087.
[34] C. Schremmer, C. Cordes, I. Klawitter, M. Bergner, C.E. Schiewer, S. Dechert, S. Demeshko, M. John, F. Meyer, Chem. Eur J. 25 (2019) 3918−3929.
[35] M.R. Anneser, G.R. Elpitiya, X.B. Powers, D.M. Jenkins, Organometallics 38 (2019) 981−987.
[36] M.R. Anneser, G.R. Elpitiya, J. Townsend, E.J. Johnson, X.B. Powers, J.F. DeJesus, K.D. Vogiatzis, D.M. Jenkins, Angew. Chem. Int. Ed. 58 (2019) 8115−8118.
[37] F. Fei, T. Lu, X.-T. Chen, Z.-L. Xue, New J. Chem. 41 (2017) 13442−13453.
[38] T. Lu, C.-F. Yang, L.-Y. Zhang, F. Fei, X.-T. Chen, Z.-L. Xue, Inorg. Chem. 56 (2017) 11917−11928.
[39] C.L. Keller, J.L. Kern, B.D. Terry, S. Roy, D.M. Jenkins, Chem. Commun. 54 (2018) 1429−1432.
[40] G.R. Elpitiya, B.J. Malbrecht, D.M. Jenkins, Inorg. Chem. 56 (2017) 14101−14110.
[41] S. Meyer, I. Klawitter, S. Demeshko, E. Bill, F. Meyer, Angew. Chem. Int. Ed. 52 (2013) 901−905.
[42] M.R. Anneser, S. Haslinger, A. Pöthig, M. Cokoja, J.-M. Basset, F.E. Kühn, Inorg. Chem. 54 (2015) 3797−3804.
[43] P.P. Chandrachud, H.M. Bass, D.M. Jenkins, Organometallics 35 (2016) 1652−1657.
[44] C. Kupper, A. Schober, S. Demeshko, M. Bergner, F. Meyer, Inorg. Chem. 54 (2015) 3096−3098.
[45] L.E. Goodrich, S. Roy, E.E. Alp, J. Zhao, M.Y. Hu, N. Lehnert, Inorg. Chem. 52 (2013) 7766−7780.
[46] C. Kupper, J.A. Rees, S. Dechert, S. DeBeer, F. Meyer, J. Am. Chem. Soc. 138 (2016) 7888−7898.
[47] S.A. Cramer, R.H. Sánchez, D.F. Brakhage, D.M. Jenkins, Chem. Commun. 50 (2014) 13967−13970.
[48] S.B. Isbill, P.P. Chandrachud, J.L. Kern, D.M. Jenkins, S. Roy, ACS Catal. 9 (2019) 6223−6233.
[49] P.J. Altmann, D.T. Weiss, C. Jandl, F.E. Kühn, Chem. Asian J. 11 (2016) 1597−1605.
[50] H.M. Bass, S.A. Cramer, A.S. McCullough, K.J. Bernstein, C.R. Murdock, D.M. Jenkins, Organometallics 32 (2013) 2160−2167.
[51] Z.S. Ghavami, M.R. Anneser, F. Kaiser, P.J. Altmann, B.J. Hofmann, J.F. Schlagintweit, G. Grivani, F.E. Kühn, Chem. Sci. 9 (2018) 8307−8314.
[52] H.M. Bass, S.A. Cramer, J.L. Price, D.M. Jenkins, Organometallics 29 (2010) 3235−3238.
[53] A.H. Mageed, B.W. Skelton, M.V. Baker, Dalton Trans. (2017) 7844−7856.
[54] H.V. Huynh, S. Guo, W. Wu, Organometallics 32 (2013) 4591−4600.
[55] B. Ballarin, L. Busetto, M.C. Cassani, C. Femoni, Inorg. Chim. Acta 363 (2010) 2055−2064.
[56] S.A. Cramer, F.L. Sturgill, P.P. Chandrachud, D.M. Jenkins, Dalton Trans. 43 (2014) 7687−7690.